



# Design of a bifunctional catalyst by alloying Ni with Ru-supported H-beta for selective hydrodeoxygenation of bisphenol A and polycarbonate plastic waste

Arjun K. Manal<sup>a,1</sup>, Ganapati V. Shanbhag<sup>b</sup>, Rajendra Srivastava<sup>a,\*,2</sup>

<sup>a</sup> Catalysis Research Laboratory, Department of Chemistry, Indian Institute of Technology Ropar, Rupnagar 140001, Punjab, India

<sup>b</sup> Materials Science Division, Poornaprajna Institute of Scientific Research, Devanahalli, Bangalore 562164, India

## ARTICLE INFO

### Keywords:

Polycarbonate plastic valorization

Ru-Ni alloy

Hydrodeoxygenation

JET fuel

Plastic waste upcycling

## ABSTRACT

The valorization of waste plastic to renewable chemicals is essential for human civilization. Bimetallic bifunctional catalysts can promote liquid-phase hydrodeoxygenation to produce liquid fuels and value-added chemicals. Ru-Ni/H-Beta bi-functional catalyst is demonstrated for the hydrodeoxygenation of bisphenol A, a monomer of polycarbonate (PC), and PC plastic waste under mild reaction conditions, afforded a complete conversion and > 90% selectivity of propane-2,2-diylidicyclohexane (P7), a JET fuel range C<sub>15</sub> cycloalkanes. The process was scaled to 2 g of plastic waste. The catalyst exhibited excellent activity (TOF-309 h<sup>-1</sup> at 0.3 h), reusability, and substrate diversity. The performance of Ru-Ni/H-Beta catalysts depends on the synergy between Ru and Ni, with the best performance observed at the Ni/Ru weight ratio of 0.5. The bimetallic Ru-Ni catalytic strategy and mechanistic understanding presented in this work provide promising insight into catalyst design and could be applied to other chemical transformations requiring efficient hydrodeoxygenation catalysts.

## 1. Introduction

A large scale of plastic production worldwide drives up fossil fuel demand and generates a massive amount of non-degradable plastic waste. The data suggests that global plastic production is around 385 million tons per year, and the estimated production of plastic in 2050 will be 30,000 million tons, which will consume 20% of the globally produced oil [1–3]. In 2018, only 9% of plastic waste was recycled, 12% was incinerated, and 79% was accumulated in landfills and natural environments [4]. The accumulated plastic waste from landfilling causes several harmful effects and environmental threats. The chemical valorization of waste plastic is one of the promising solutions to make a plastic waste-free and carbon-neutral society. Hydrogenolysis/hydrodeoxygenation is an energy-efficient and beneficial method that transforms plastic waste into high-value chemicals and fuels [5,6].

Polycarbonate (PC) is a preeminent engineering plastic with the fastest growth rate among the five primary engineering plastics due to its exceptional physicochemical properties. Polycarbonate (PC) is

widely used in the automotive, safety equipment, construction, electronics, and medicinal industries [7–9]. However, studies show that the monomer of PC, such as bisphenol A (BPA) can be leached from the PC products, such as food packaging and baby bottle, and cause several harmful effects on human health [10–12]. Nevertheless, the PC production capacity continuously increased and is estimated to be ~ 6 million tonnes/year. So, it is necessary to recycle PC plastic waste responsibly [13]. Therefore, researchers are exploring green and sustainable recycling processes. As a result, chemical recycling is a promising process that has drawn much attention in recent years. Numerous methods have been devoted to PC upcycling high-value chemicals, including pyrolysis, hydrocracking, liquefaction, alcoholysis, aminolysis, hydrolysis, and glycolysis [14–20]. Nang Li et al. and a co-worker first reported the hydrodeoxygenation of BPA to propane-2,2-diylidicyclohexane, a jet fuel range C<sub>15</sub> bi-cycloalkanes over 5% Pt/C and H-Beta zeolite catalyst [21]. Propane-2,2-diylidicyclohexane is an important and highly demanded transportation fuel, which has a higher density (0.92 g ml<sup>-1</sup>) and volumetric net heat of combustion (NHOC - 39.5 MJ L<sup>-1</sup>) than the currently used JP-8 JET fuel. Later, the same group

\* Corresponding author.

E-mail address: [rajendra@iitrpr.ac.in](mailto:rajendra@iitrpr.ac.in) (R. Srivastava).

<sup>1</sup> ORCID: 0000-0001-9864-6966

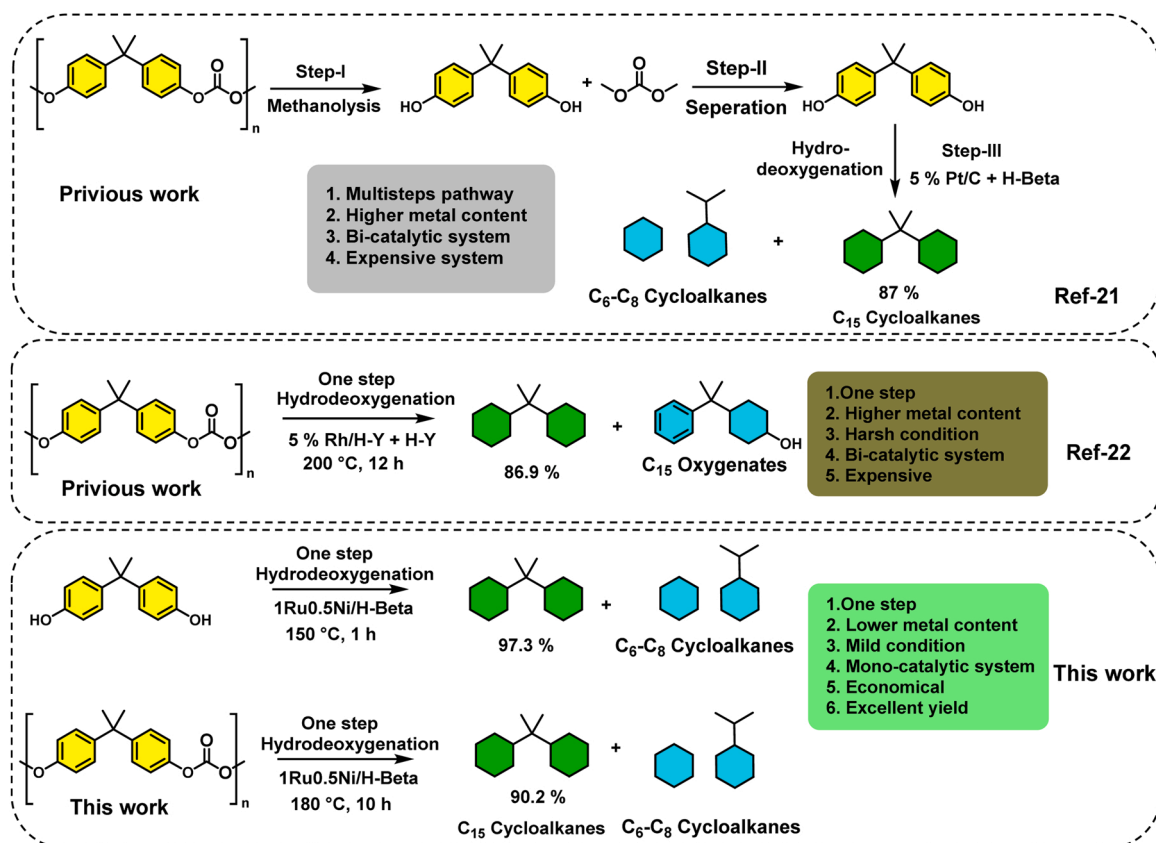
<sup>2</sup> ORCID: 0000-0003-2271-5376

reported a direct hydrodeoxygenation of PC to C<sub>15</sub> bicycloalkanes using 5% Rh/H-Y with H-Y zeolite catalyst at 200 °C for 12 h [22]. Nevertheless, both works revealed that the bi-catalytic system (comprising two catalysts) greatly worked for the PC transformation. Compared to the bi-catalytic system, the mono-catalytic (single catalyst) system would be beneficial due to the ease of catalyst synthesis, easy recovery and recycling, and a comparatively simpler infrastructure for commercialization. It is difficult to activate BPA and PC over a mono-catalytic system under mild reaction conditions, and significant challenges exist in controlling the selectivity towards propane-2,2-diylidicyclohexane due to a lack of literature and structure-activity relationship study. As per our knowledge, there is no report on a mono-catalytic system for direct hydrodeoxygenation of BPA and PC to bicycloalkanes, which remains challenging Scheme 1.

During the past decades, solid acid catalysts such as aluminosilicate zeolites (e.g., ZSM-5, Beta, Y Zeolite) combined with metals (Pt, Pd, Ru, etc.) have been employed to catalyze the hydrodeoxygenation (HDO) of phenolic compounds to cycloalkanes through the cascade hydrogenation/hydrogenolysis over metal (Pt, Pd, Ru, etc.) and dehydration over solid acid sites of bi-functional metal/acid catalysts [23,24]. Among them, the less expensive Ru-based solid acid catalyst exhibited higher selectivity towards cyclic hydrocarbon than other metal-based catalysts [25]. More recently, researchers prepared a Ru-based bimetallic, bi-functional solid acid catalyst with the aim to fine-tune and increase the HDO activity of phenolic and reduce the catalyst cost. The bimetallic or bifunctional catalyst usually shows different chemical and electronic properties that can be changed by forming the heteroatom bond, which differs from its parent metal and has gained significant academic and industrial interest [26]. Additionally, bimetallic catalysts may form heterogeneous metal-metal bonds, which cause a change in orbital overlapping and strain effect that can alter the geometric structure of the catalyst [27,28]. Many researchers explored the interaction between

metal-metal species, substrate adsorption properties, and the synergistic effect of bimetallic catalysts on catalytic performance. Recently researchers examined the efficient zeolite-supported Ru-M (M= Fe, Cu, Ni, & Zn) catalysts for total hydrodeoxygenation of lignin phenolics, which exhibited excellent catalytic activity [29–32]. Encourage by these studies, herein we report a zeolite Beta supported Ru-based bi-metallic or bi-functional catalysts for complete HDO of BPA and PC under mild reaction conditions.

In this contribution, a mono-catalyst system is demonstrated for hydrodeoxygenation of bisphenol A (BPA) and polycarbonate (PC) plastic waste to the selective synthesis of propane-2,2-diylidicyclohexane (P7), a C<sub>15</sub> polycycloalkane as a high-density JET fuel range chemical. Herein, a highly dispersed Ru-Ni bimetallic alloy supported H-Beta, has been designed, prepared, and employed for the selective HDO of BPA to C<sub>15</sub> poly-cycloalkanes (P7) with an excellent yield of 97.3%. In addition, the role of a highly dispersed Ru-Ni phase & Ru NPs with optimized Ni/Ru weight ratio, and the synergetic effect of Ru-Ni alloy unravel the reaction pathway, substrate activation, and product selectivity in the HDO of BPA and PC. Extensive characterization techniques were employed to thoroughly investigate the inherent structural properties of Ru and Ni and the interactions between these two elements. The relationship between the structural characteristics and the catalytic activity was also studied to establish a comprehensive structure-activity relationship. It could be the first mono-catalytic system that achieved the upgrading of PC waste into bi-cycloalkanes (P7) selectively. Moreover, this work opens up a new perspective on the HDO of PC and BPA and provides more possibilities for their applications in other important reactions, such as the HDO of lignin bio-oils.



**Scheme 1.** Strategy for synthesizing jet fuel range propane-2,2-diylidicyclohexane (P7) by hydrodeoxygenation of BPA and PC.

## 2. Experimental section

### 2.1. Catalyst preparation and characterizations

The zeolite H-Beta (Si/Al=12.5) supported monometallic and bimetallic catalysts were prepared by a one-pot impregnation method, followed by a reduction in 10% H<sub>2</sub>/Ar mixture. The details are provided in [Supporting Information](#). The details of various characterization methods and analytical instruments are also provided in [Supporting Information](#).

### 2.2. Catalytic process for the HDO of bisphenol A and polycarbonate waste

The hydrodeoxygenation of the polycarbonate model compounds (Bisphenol A) and polycarbonate waste was carried out in a stainless-steel high-pressure Parr reactor. All the details of the reactions, processing of polycarbonate waste, details of analysis, and quantification methods are provided in the [Supporting Information](#) section.

## 3. Result and discussion

### 3.1. Physicochemical characterization of catalysts

The XRD patterns of the catalysts were recorded in  $2\theta = 5-80^\circ$  (Fig. 1 (a, b) and Fig. S1). The XRD patterns of all catalysts depict two diffraction peaks at  $2\theta \sim 8^\circ$  and  $\sim 22.5^\circ$ , ascribed to the crystalline BEA framework structure of H-Beta zeolite, indicating metal impregnation has no significant effect on the BEA framework structure. Besides, the low concentration and high dispersion of metal nanoparticles (NPs) could obscure the metal NPs observation from the XRD pattern. The XRD pattern of 1Ru/H-Beta shows that a broad peak at  $2\theta = 43.7^\circ$  corresponding to NaAlSiO<sub>4</sub> (JCPDS 33-1203) in H-Beta zeolite was slightly expanded towards the lower  $2\theta = 43.4^\circ$  attributed to Ru (002) and (101) planes, corresponding the hexagonal closed packed (hcp) structure of Ru nanoparticle (JCPDS card No. 00-006-0663) [33]. The XRD pattern of 1Ni/H-Beta shows the diffractions at  $2\theta = 44.5^\circ$  and  $51.9^\circ$ , attributable to Ni (111) and (200) planes, overlapped with the fcc structure of Ni NPs (JCPDS card No. 01-087-0712) [34]. The comparison of XRD

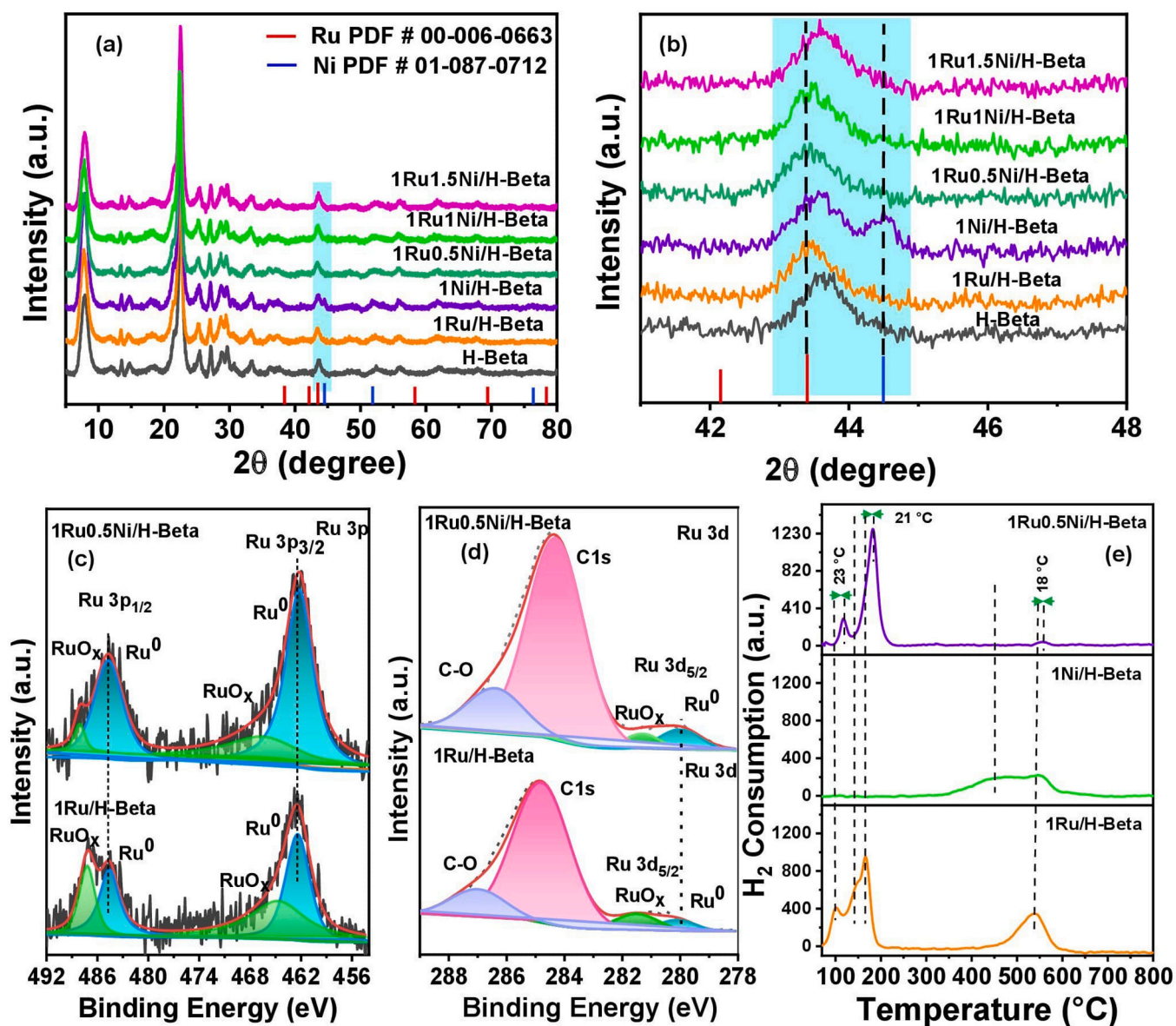


Fig. 1. PXRD patterns of mono-metallic and bi-metallic catalysts (a); The main peak corresponding to alloy enlarged from the highlighted region of fig. a (b); Deconvoluted XPS spectra of Ru 3p and Ru 3d of 1Ru/H-Beta and 1Ru0.5Ni/H-Beta (c-d). H<sub>2</sub>-TPR profiles of different catalysts (e).

diffractions of single metal supported Beta (1Ru/H-Beta and 1Ni/H-Beta) with bimetallic Ru-Ni/H-Beta catalysts shows the diffraction peaks at  $2\theta = 43.4^\circ$ , and  $44.5^\circ$  for Ru (002), (101) and Ni (200) planes were merged and resulted in a broader diffraction peak at  $2\theta = 43.6\text{--}43.9^\circ$  corresponding to Ru-Ni alloy NPs (Fig. 1a,b) [35]. The molar ratio of Ru/Ni for 1Ru0.5Ni/H-Beta was 1.28 (Table 1). The characteristic peak of Ni (111) was not separately observed, suggesting that Ni formed a solid solution with Ru. The XRD patterns of the bimetallic Ru-Ni/H-Beta catalysts shifted towards higher  $2\theta$  with increasing the Ni content in the catalyst, suggesting the successful alloying of Ni with Ru (Fig. 1b) [35,36].

The formation of Ru-Ni alloy and the presence of Ru<sup>0</sup>, RuO<sub>x</sub> domain in 1Ru/H-Beta and 1Ru0.5Ni/H-Beta was consolidated using X-ray photoelectron spectroscopy. The surface profiles of the 1Ru/H-Beta and 1Ru0.5Ni/H-Beta confirmed Ru, O, Si, Al; and Ru, Ni, Si, O, and Al elements, respectively (Fig. S2). The element's binding energy was corrected using C 1 s (284.6 eV) as a reference [37]. Fig. 1c,d illustrates the core level XPS profile of Ru 3p, which displays two doublets corresponding to Ru 3p<sub>3/2</sub> and Ru 3p<sub>1/2</sub>. The deconvolution of the Ru 3p spectrum for 1Ru0.5Ni/H-Beta utilizing curve fitting methods reveals two peaks at binding energies of 462.1 eV and 484.9 eV, indicating the metallic Ru<sup>0</sup>. These peaks exhibit 0.4–0.6 eV lower binding energy than the Ru 3p<sub>3/2</sub> and Ru 3p<sub>1/2</sub> peaks of the 1Ru/H-Beta catalyst, confirming the strong interaction between Ru and Ni and the electron transfer from Ni to Ru, caused by the lower electronegativity of Ni metal (Ru,  $\chi = 2.2$ ; Ni,  $\chi = 1.9$ ). Furthermore, the area under the curve of RuO<sub>x</sub> peaks observed at 467.0 eV and 488.4 eV revealed that the 1Ru/H-Beta has a higher concentration of RuO<sub>x</sub> species than 1Ru0.5Ni/H-Beta, indicating Ru has strong interaction with H-Beta in 1Ru/H-Beta and Ru was difficult to reduce, even at 500 °C, which is in agreement with H<sub>2</sub>-TPR results (discussed later). The deconvoluted Ru 3d<sub>5/2</sub> spectrum of 1Ru0.5Ni/H-Beta exhibited doublets at 279.8 eV and 281.5 eV binding energies assigned to Ru<sup>0</sup> and RuO<sub>x</sub>, which are also situated at the lower binding energies than 1Ru/H-Beta and consisted with the literature reports [38]. Additionally, the Ru<sup>0</sup>/RuO<sub>x</sub> ratio was calculated for 1Ru0.5Ni/H-Beta to be ~8.6, which was higher than 1Ru/H-Beta (~2.0).

The lower binding energy and higher Ru<sup>0</sup> content in the 1Ru0.5Ni/H-Beta indicate the strong electronic interaction between the Ru and Ni and electron transfer from the Ni to Ru by their proximity, suggesting the formation of the metallic alloying structure in 1Ru0.5Ni/H-Beta and results are consistent with the XRD and TEM results (discussed later). The higher fraction of Ru<sup>0</sup> further confirmed that a higher concentration of metallic alloy was present in the catalyst.

H<sub>2</sub>-TPR profiles were recorded for metal-impregnated samples heated at 500 °C for 4 h to investigate the reduction behavior of mono-metallic 1Ru/H-Beta, 1Ni/H-Beta, and bimetallic 1Ru0.5Ni/H-Beta before the reduction of materials (Fig. 1e). The H<sub>2</sub>-TPR profile of 1Ru/H-Beta exhibited two peaks at lower temperatures 94 °C and 162 °C, which are attributed to Ru<sup>4+</sup> to Ru<sup>2+</sup> and Ru<sup>2+</sup> to Ru<sup>0</sup> reduction,

respectively. A broad peak at a high temperature of 540 °C is attributed to reducing RuO<sub>x</sub> species (having strong interactions with H-Beta) to Ru<sup>0</sup> (total H<sub>2</sub>-consumption was 0.144 mmol/g cat.) [39]. The H<sub>2</sub>-TPR profile of 1Ni/H-Beta exhibited two less-distinguishable peaks at 450 °C and 550 °C, which are attributed to isolated NiO to Ni<sup>0</sup> NPs and NiO having strong interaction with H-Beta to Ni<sup>0</sup> NPs reduction, respectively (H<sub>2</sub>-consumption was 0.105 mmol/g). In contrast, the H<sub>2</sub>-TPR profile of the bimetallic 1Ru0.5Ni/H-Beta catalyst displayed sharp reduction peaks at lower temperatures of 117 °C and 183 °C (shifted to 23 °C and 21 °C higher temperature than 1Ru/H-Beta). The reduction peak maximum shift towards a higher temperature than 1Ru/H-Beta, suggesting a strong interaction between Ru & Ni atoms, indicating the formation Ru-Ni alloy [40]. Additionally, another reduction peak with a peak maximum at 558 °C (shifted by 18 °C higher temperature than 1Ru/H-Beta) further suggests the formation of Ru-Ni alloy particles that strongly interacted with the H-Beta (H<sub>2</sub>-consumption was 0.276 mmol/g). The area under the curve of H<sub>2</sub>-TPR peaks indicates that the ~90% Ru species of 1Ru0.5Ni/H-Beta was reduced at lower temperatures, which aligns with the XPS results (Table 2).

To further investigate the formation of the Ru-Ni bimetallic alloy, HR-TEM images were captured, and the corresponding energy dispersive X-ray (EDX) spectrum was recorded. The HR-TEM images show the average 1Ru0.5Ni alloy NPs size of 3.42 nm, and the alloy NPs are located on the external surface of H-Beta (Fig. 2). The % metal dispersion was calculated to be ~29% (Eq. S1). The lattice fringes with the interplanar distance of 0.204 nm, 0.221 nm, and 0.232 nm are correlated to (101), (111), and (100) planes, respectively, for Ru in Ru-Ni alloy NPs. Similarly, the interplanar distance of 0.173 is attributable to the (200) plane of Ni in the Ru-Ni alloy for 1Ru0.5Ni/H-Beta. The observed d spacing in this catalyst is different from the crystal plane of Ru 0.206 nm (101), 0.220 nm (111), 0.234 nm (100) for Ru NPs and Ni 0.176 nm (200) for Ni NPs, suggesting the formation of a solid crystal structure of metallic Ru-Ni alloy NPs [36,41]. The lattice fringe and corresponding FFT results exhibited typical characteristic phases of Ru-Ni alloy (Fig. 2e–j). The results are consistent with the results obtained from XRD and XPS. Further, the SAED pattern of 1Ru0.5Ni/H-Beta reveals a series of circles with multiple spots, attributed d-spacing values corresponding to the (111), (200), (002), and (100) planes, indicating the formation of Ru-Ni alloy and consistent with HR-TEM (Fig. S3 and Table S2). The energy dispersive X-ray (EDX) mapping shows Si, Al, and O-rich H-Beta zeolite with a homogeneous distribution of Ru-Ni NPs on the H-Beta surface (Fig. 2l). The EDX mapping images (Fig. 2k–p) show Ru and Ni are located at the same position, which also evidenced the formation of Ru-Ni bimetallic alloy (Fig. 2o, p).

The N<sub>2</sub> adsorption-desorption isotherms were recorded to determine the surface area and pore volume of all the synthesized materials. (Table 1 and Fig. S4). The adsorption at lower p/p<sub>0</sub> shows a type II isotherm of H-Beta with an H4 hysteresis loop, confirming that H-Beta possesses microporosity and inter-particle mesoporosity. The adsorption

**Table 1**  
Physiochemical properties of the synthesized catalyst.

Catalyst	Relative crystallinity (%) <sup>a</sup>	Ru Content (wt%) <sup>b</sup>	M Content (wt%) <sup>b</sup>	Ru/M Molar ratio	BET Surface area (m <sup>2</sup> /g) <sup>c</sup>			Pore volume (cm <sup>3</sup> /g) <sup>d</sup>	
					Micro-pore area	External surface area	Total surface area	Micro-pore	Total
H-Beta	92	-	-	-	317	273	590	0.17	0.89
1Ru/H-Beta	89	0.97	-	-	310	267	577	0.15	0.87
1Ni/H-Beta	91	-	0.98	-	287	256	544	0.15	0.84
1Ru0.5Ni/H-Beta	88	0.96	0.44	1.28	305	233	538	0.15	0.85
1Ru0.5Co/H-Beta	87	0.92	0.42	1.27	300	224	524	0.15	0.78
1Ru0.5Cu/H-Beta	90	0.96	0.43	1.40	287	234	521	0.14	0.79
1Ru0.5Zn/H-Beta	85	0.95	0.48	1.28	300	278	579	0.15	0.82
1Ru1.5Ni/H-Beta	86	0.94	1.41	0.38	306	192	498	0.14	0.77

<sup>a</sup> Determined by XRD analysis, <sup>b</sup> Determined by MP-AES analysis, <sup>c</sup> Micropore surface area calculated by t-plot method, specific surface area calculated by BET equation, <sup>d</sup> Micropore volume was determined using the t-plot method.



**Table 2**Chemical state, H<sub>2</sub> consumption, and H<sub>2</sub> desorption value of the catalysts.

Catalyst	Relative % of active species		H <sub>2</sub> consumption mmol/g <sub>cat</sub> <sup>b</sup>	H <sub>2</sub> /M (mmol/ mmol) <sup>b</sup>	Amount of H <sub>2</sub> desorbed mmol/g <sub>cat</sub> <sup>c</sup>	H <sub>2</sub> /M (mmol/ mmol) <sup>c</sup>	Total acid conc. (μmol NH <sub>3</sub> /g <sub>cat</sub> ) <sup>d</sup>
	Ru <sup>0</sup>	RuO <sub>x</sub>					
H-Beta	-	-	-	-	-	-	87.3
1Ru/H-Beta	66.3	33.7	0.144	1.51	12.41	129.3	104.8
1Ni/H-Beta	-	-	0.105	0.63	10.52	63.0	104.8
1Ru0.5Ni/H-Beta	89.6	10.4	0.276	1.63	11.45	67.7	115.0

<sup>a</sup>Determined from XPS; <sup>b</sup>Calculated from H<sub>2</sub>-TPR; <sup>c</sup>Calculated by H<sub>2</sub>-TPD; <sup>d</sup>Calculated by NH<sub>3</sub>-TPD

behavior of metal NPs embedded H-Beta was comparable to that of parent H-Beta, albeit with reduced adsorption volume. The decrease in external surface area and pore volume observed in 1Ru/H-Beta suggests the decoration of Ru NPs on the external surface of the H-Beta. Ni-decorated Beta zeolite exhibited a reduced surface area and pore volume than H-Beta, indicating the formation of Ni NPs on the surface of H-Beta (Table 1). The bimetallic RuM/H-Beta catalysts also showed a reduction in surface area and pore volume, which is attributed to the formation of NPs on the external surface of the H-Beta zeolite.

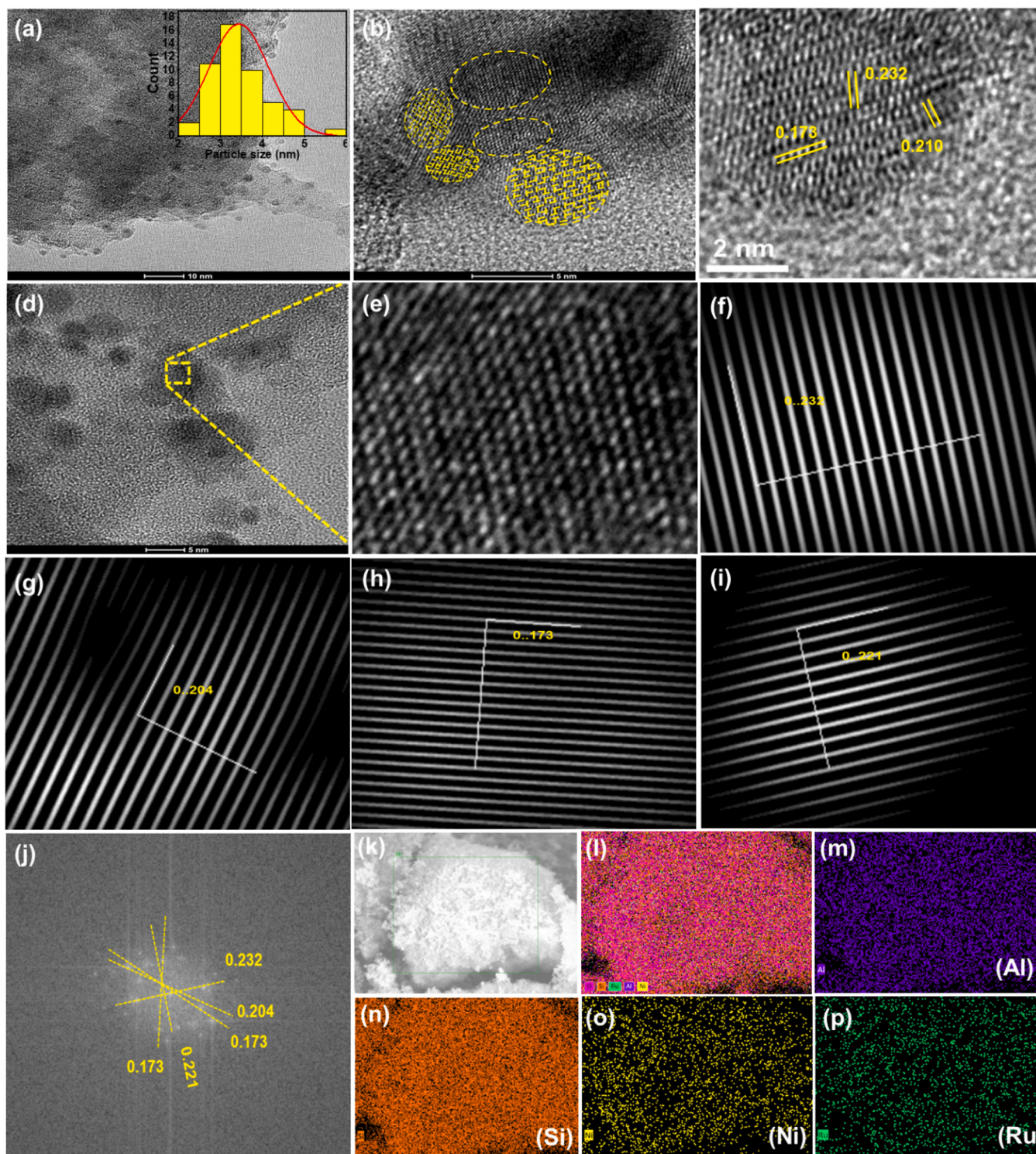
Hydrogen desorption from the catalyst was analyzed using temperature-programmed desorption (H<sub>2</sub>-TPD). It is known that the active metal dissociative adsorbs H<sub>2</sub> and then transfers it to the adsorbed reactants through the metal-support interface [42]. Fig. S5 shows two desorption features at 75–400 °C and 450–700 °C, ascribed to the chemisorbed hydrogen at lower temperatures and spillover hydrogen at higher temperatures, respectively [43]. The dissociative adsorbed hydrogen migrates through a spillover process facilitated by the acid sites of zeolites. The spillover hydrogens transport through (H<sup>+</sup>/e<sup>-</sup>). H<sup>+</sup> migrates through Brønsted acidic sites of H-Beta, and e<sup>-</sup> migrates through Lewis acid sites [44]. The total amount of desorbed hydrogen is provided in Table 2. The hydrogen desorption from the Ru/H-Beta catalysts was higher than Ni/H-Beta and Ru-Ni/H-Beta (Fig. S5 and Table 2), indicating that Ru has a higher capacity to adsorb hydrogen on sites. When Ni was introduced to the Ru/H-Beta catalyst, the desorption amount of hydrogen decreased, suggesting that Ni partially blocked the Ru sites and lowered its ability to adsorb hydrogen. Therefore, it can be concluded that the dissociative absorption of hydrogen is dominant over Ru sites in the bimetallic system.

The rate of HDO reactions also depends on the acidity of the catalysts. The temperature-programmed desorption of NH<sub>3</sub> was performed to estimate the acidity of catalysts (Table S3). The NH<sub>3</sub> desorption at 110–320 °C is associated with the weakly adsorbed NH<sub>3</sub> molecules from weak acidic sites of catalysts, and the desorption at 420–600 °C is related to strong acidic sites of catalysts. Fig. S6 shows that the concentrations of higher acidic strength sites are more for 1Ru/H-Beta and 1Ni/H-Beta than H-Beta, suggesting that Ru or Ni sites are also the sites for NH<sub>3</sub> adsorption. Furthermore, higher-strength acid sites are present in 1Ni/H-Beta than 1Ru/H-Beta. The TPD peak of 1Ru0.5Ni/H-Beta is intermediate between 1Ru/H-Beta and 1Ni/H-Beta, indicating a strong interaction between Ru and Ni. Furthermore, 1Ru0.5Ni/H-Beta exhibited the highest uptake of NH<sub>3</sub> per gram of catalyst than other monometallic and bi-metallic catalysts synthesized in this study (Fig. S6). Additionally, pyridine-adsorbed FT-IR spectra were recorded to investigate the type of acid sites of catalysts (Fig. S7). The intense band at 1445 cm<sup>-1</sup> is assigned to the Lewis acid sites of the catalysts, while the broad bands at 1540 cm<sup>-1</sup> and 1635 cm<sup>-1</sup> are attributed to the Brønsted acid sites of the catalysts [45]. Moreover, the combination of Lewis and Brønsted acid sites peak is observed at 1482 cm<sup>-1</sup>. In addition, the vibration peak 1595 cm<sup>-1</sup> corresponding to H-bonded pyridine is observed [46]. The results indicate that all catalysts exhibited Lewis and Brønsted acid sites, and no changes were observed in the nature of acid sites of H-Beta upon metal decoration.

### 3.2. HDO of bisphenol A

The catalytic hydrodeoxygenation of BPA, a typical polycarbonate monomer, was investigated at 150 °C, 3.0 MPa H<sub>2</sub> gas for 1 h using monometallic and bimetallic supported H-Beta catalysts. The structure of H-Beta and the BPA HDO transformation is shown in Scheme S2. All synthesized catalysts in this study were tested for HDO of BPA, and the results are summarised in Fig. 3 and Table S5. It was observed that the Ru contents in the monometallic catalyst influenced the reaction pathway in the HDO process and altered the product distribution. The selectivity of propane-2,2-diylidicyclohexane (designated as P7, Fig. 3a) follows the order 1Ru/H-Beta > 0.5Ru/H-Beta > 1.5Ru/H-Beta > 2.0 Ru/H-Beta. When the Ru loading was increased from 1 wt% to 2.0 wt%, BPA conversion was increased, while the selectivity to desired product P7 was decreased (Table S5). Based on the results obtained, it can conclude that the higher Ru content activated the Csp<sup>2</sup>-Csp<sup>3</sup> bond leading to the decomposition of BPA to form C6-C9 lower range hydrocarbon (i.e., Low-density hydrocarbons P3-P6) (Fig. 3a) [47]. Propane-2,2-diylidicyclohexane (P7) is a highly demanded transportation fuel because of its higher density and net heat of combustion value than the currently used JET and Rocket fuels (Table S6, Table S7).

The GC-MS chromatogram of the reaction mixture is shown in Fig. S8 and S9, which corresponds to P7 and the other C-15 oxygenates and degraded products, such as C6-C9 oxygenates and hydrocarbons. Ru-based bimetallic catalysts have been reported to exhibit better activity than the monometallic catalyst for HDO of lignin-derived phenolics and reduce the catalyst cost [48–50]. Bimetallic catalysts form heterogeneous metal-metal bonds, which cause a change in the orbitals overlap and alter the geometric structure of the catalyst. Therefore, to enhance the Ru/H-Beta efficiency towards BPA conversion and P7 product selectivity, the bimetallic systems 1RuM/H-Beta (M= Co, Ni, Cu, Zn) were prepared. The most selective 1Ru/H-Beta was chosen for further catalyst modification, and other inexpensive metals (M) loading was varied from 0.25 wt% to 1.5 wt%. Although BPA conversion was above 80%, the bimetallic 1Ru 0.5 M/H-Beta catalysts showed higher HDO activities than monometallic 1Ru/Beta (Table S5, Entries 6–14). Especially in the case of 1Ru0.5Ni/H-Beta, the best result was achieved, which afforded a complete conversion of BPA and 97.3% selectivity of P7 (Fig. 3b & Table S5, Entry 6). Based on the Ru content, the TOFs for BPA conversion were calculated at a lower BPA conversion (<50%). Fig. 3c displayed a TOFs of BPA vs the selectivity of P7 over different catalysts at 0.3 h. The results indicate that the Ru-Ni/H-Beta bimetallic catalyst has a higher TOF than the monometallic Ru/H-Beta and Ni/H-Beta catalysts. Specifically, the 1Ru0.5Ni/H-Beta catalyst exhibited the highest P7 selectivity (92%) and a TOF of 309 h<sup>-1</sup> at 0.3 h, which is three times higher than recently reported catalysts, [21,22] demonstrating the superiority of the Ru–Ni bimetallic catalysts. The TOFs of BPA over all the investigated catalysts under the optimized reaction conditions after 1 h are provided in Table S5. Further, the product selectivity was plotted for different catalysts at nearly similar conversion levels (~ 45–48%), indicating the highest selectivity of 1Ru0.5Ni/H-Beta even at lower reaction time than others (Fig. S10). It is reported that bimetallic Ru-Ni catalyst enriches the surface and enhances the metal dispersion, thereby enhancing the activity and stability of the Ru-Ni bimetallic catalyst [51]. Herein, a bimetallic Ru-Ni formed an

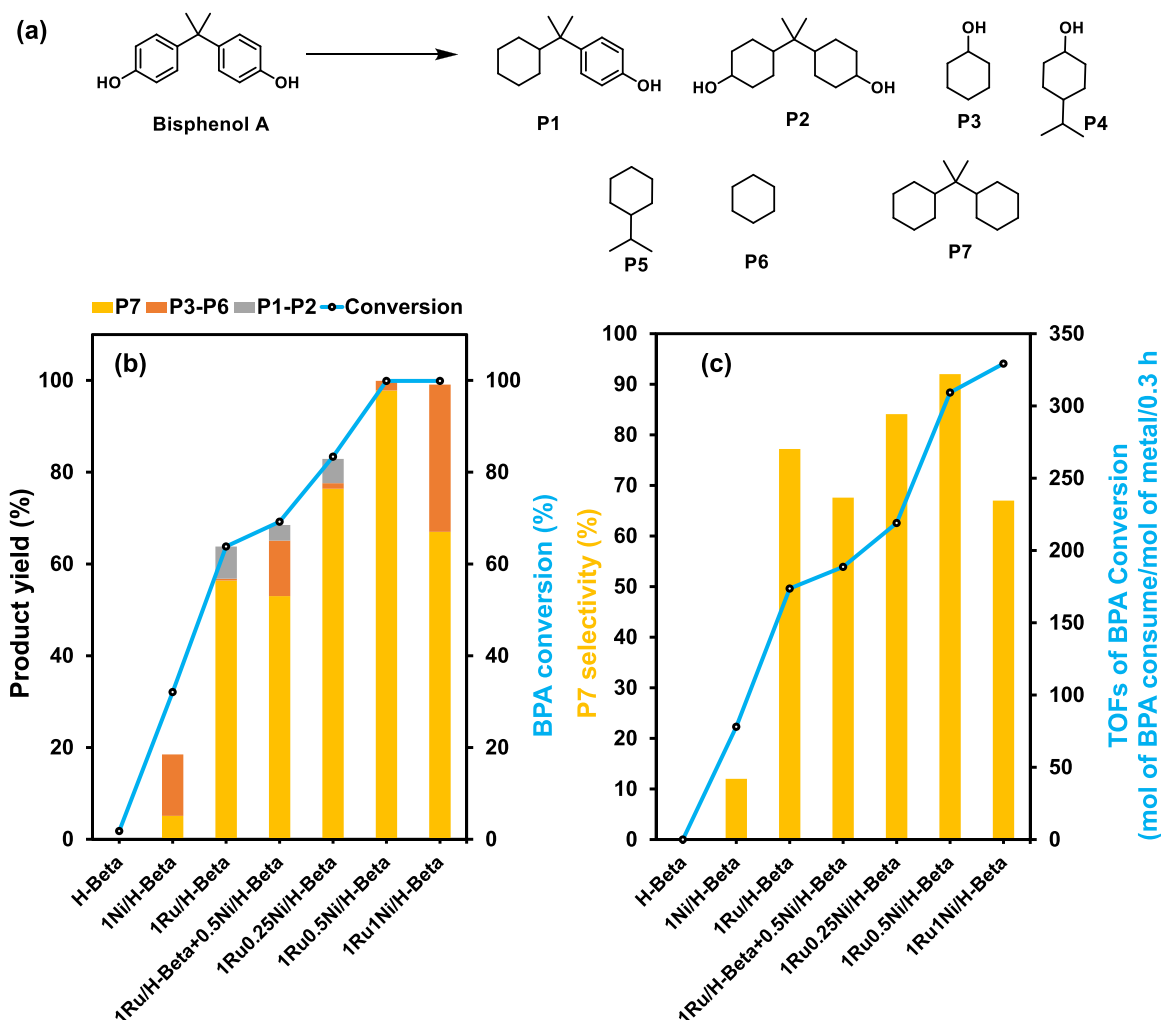


**Fig. 2.** The structural properties of the 1Ru0.5Ni/H-Beta catalyst. (a-e) HR-TEM images and average particle size of the catalyst; (f-j) the FFT electron diffraction patterns of HR-TEM image (d); (k-p) the images of EDS mapping of 1Ru0.5Ni/H-Beta catalyst.

alloy confirmed by XRD, XPS, HR-TEM,  $H_2$ -TPR, and  $H_2$ -TPD analysis. The strong interaction between Ru-Ni allows the preferential adsorption and activation of the substrates, which is responsible for the higher activity of Ru-Ni alloy than the monometallic Ru and Ni, confirmed by the DRIFT and kinetic experiments (discussed below). The Ni/Ru weight ratio influenced the P7 selectivity, which shows a volcano-type curve between yield and TOF for forming P7 (Fig. S11). Several experiments were conducted under optimized reaction conditions to investigate the

synergy and optimum ratio between Ru and Ni. 1Ni/H-Beta afforded 32.1% BPA conversion, and 84% selectivity for C-C bond cleaved monocyclic oxygenated phenolics was obtained. A physical mixture of the 1Ru/H-Beta and 0.5Ni/H-Beta afforded similar BPA conversion to 1Ru/H-Beta, but selectivity was similar to Ni/H-Beta catalyst (67% BPA conversion, 68% selectivity for mono-cycloalkanes, and 26% of P7). The excess Ni content in the catalyst (1Ru1.25Ni/H-Beta) afforded the complete conversion of BPA and 46.8% selectivity of P7 and 53% of





**Fig. 3.** The catalytic evaluation for the HDO of BPA and the product distribution of BPA during the HDO reaction (a). Catalyst activity and product distribution (b), Reaction conditions: 0.228 g BPA (1.0 mmol), 0.05 g catalyst, 3.0 MPa H<sub>2</sub>, 800 rpm agitation speed, 10 ml decane, 150 °C, and 1 h. P7 selectivity and TOFs of BPA conversion at time 0.3 h (c), Reaction conditions: 0.228 g BPA (1.0 mmol), 0.05 g catalyst, 3.0 MPa H<sub>2</sub>, 800 rpm agitation speed, 10 ml decane, 150 °C, and 0.3 h. TOFs for BPA conversion were calculated by (mol<sub>BPA</sub> consumed/mol<sub>Ru</sub> metal/0.3 h).

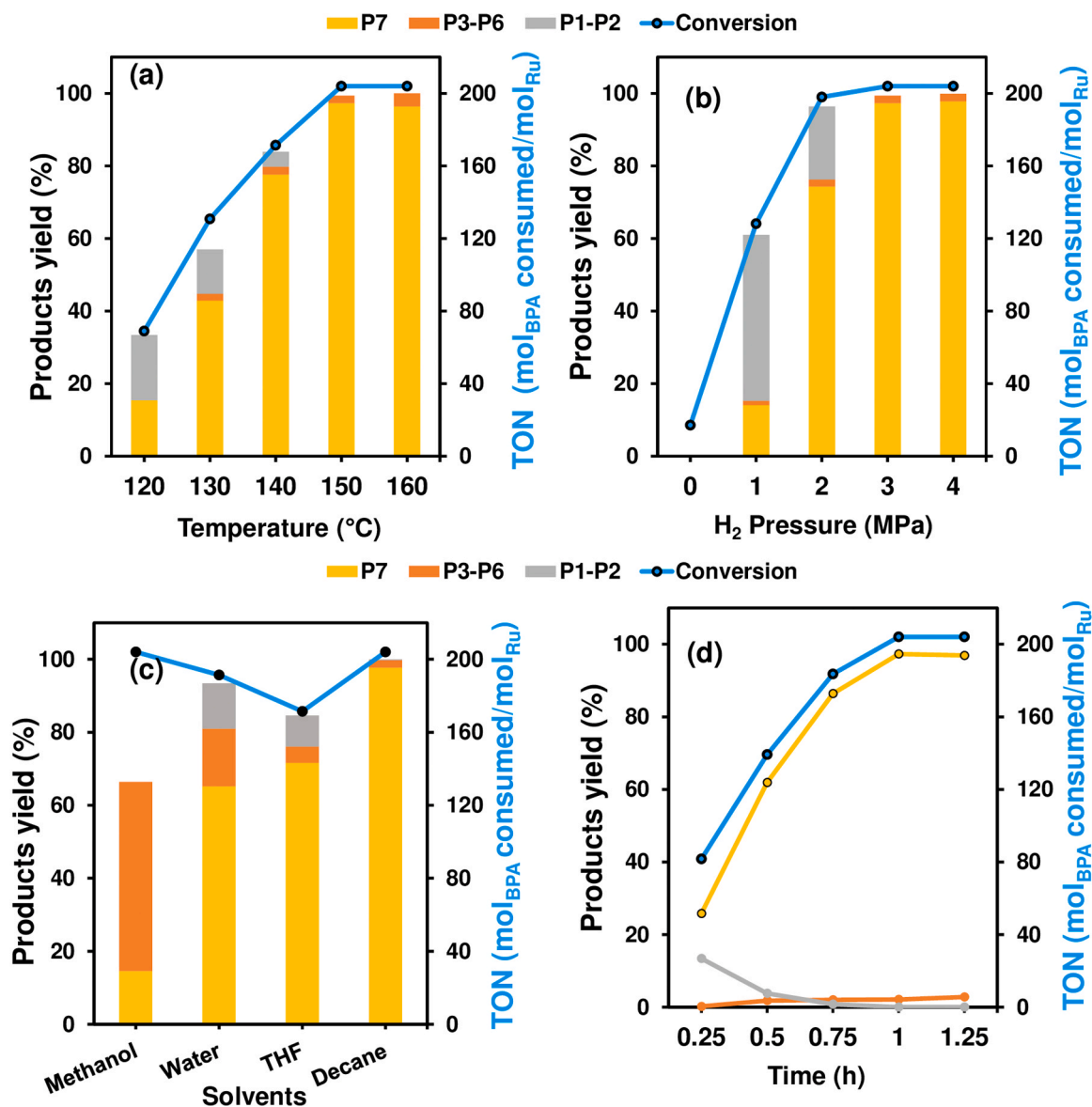
P3-P6 (Table S5). The results suggest that dissociative adsorption of hydrogen on Ru sites facilitates the reduction of the aromatic ring to the desired product, and Ni sites effectively cleaved Csp<sup>2</sup>-Csp<sup>3</sup> bond by the strong adsorption of BPA to the corresponding phenolic, which indicates that the Ru-Ni alloyed NPs structure is beneficial for improving the activity and selectivity than monometallic metal NPs. An excess amount of Ni content in the bimetallic catalyst form Ru-Ni alloy and Ni NPs, which partially block the active Ru metal sites and cleave Csp<sup>2</sup>-Csp<sup>3</sup> and C-O bond to form monocyclic cycloalkanes selectively, which are in good agreement with low selectivity of P7 with the higher Ni content (1Ru1.25Ni/H-Beta) and the selectivity resembles with a monometallic Ni/H-Beta catalyst. Ni-supported zeolites are reported for selective cleavage Csp<sup>2</sup>-Csp<sup>3</sup> bond of isopropyl phenol to phenol [52]. The catalytic data over mono and bimetallic catalysts suggests that the optimum amount of Ni formed an alloy with Ru, and the interfacial site of Ru-Ni alloy is greatly responsible for the selective HDO of BPA to P7. Additionally, this catalytic system underwent rigorous evaluation for the HDO of important compounds of lignin bio-oils (model compounds), such as phenol, *p*-cresol, and eugenol, yielding exceptional outcomes under mild conditions (Table S9–S11, Table 4). These outcomes suggest promising opportunities to broaden the scope of substrate versatility and applicability of this catalytic system.

The reaction conditions such as temperature, hydrogen pressure, solvent, and reaction time were varied to achieve the higher conversion

of BPA and P7 selectivity over 1Ru0.5Ni/H-Beta (Fig. 4). The temperature was increased from 120 °C to 150 °C at an initial hydrogen H<sub>2</sub> pressure of 3.0 MPa, catalyst-to-substrate mass ratio of 1:4.5, 1 h, in decane. With the increase in the temperature, BPA conversion increased from 33.8% to 99.9% (TON rose from 69 to 204) and P7 yield rose from 15.4% to 97.4%, and alcohols (P1-P4) yield decreased from 18.4% to 0.2% (Fig. 4a and Fig. S12 a). When the temperature was further increased from 150 °C to 160 °C, a decrease in P7 selectivity was recorded. However, at 160 °C, nearly complete BPA conversion was observed in 0.4 h (P7 selectivity 83%). The higher P7 selectivity was obtained at 150 °C; thus, it was chosen for further optimization.

The influence of H<sub>2</sub> pressure on BPA HDO is shown in Fig. 4b. The influence of H<sub>2</sub> pressure on BPA conversion and product selectivity is also presented in Fig. S12b. Without H<sub>2</sub>, only 8.4% BPA conversion was observed, and only phenolics were obtained. At 1.0 MPa H<sub>2</sub> pressure, 62.8% BPA conversion and 14.1% P7 yield were obtained. The higher yield of partial hydrogenated polycyclic alcohol suggests that a higher H<sub>2</sub> pressure was required to reduce the benzene ring. When the H<sub>2</sub> pressure increased from 1.0 MPa to 2.0 MPa, BPA was completely converted, but the P7 yield was still 74.3%. At a 3.0 MPa H<sub>2</sub> pressure, a higher yield of P7 (97.3%) was obtained with complete conversion of BPA. No significant change in BPA conversion and P7 yield was observed above 3 MP; thus, it was chosen as the optimum pressure.

The choice of solvent for the HDO significantly influences the



**Fig. 4.** Evaluation of reaction parameters to obtain higher catalytic activity towards BPA conversion and P7 yield. (a) Temperature (Reaction conditions: 0.228 g BPA (1.0 mmol), 0.05 g catalyst, 3.0 MPa H<sub>2</sub>, 800 rpm agitation speed, 10 ml decane, and 1 h; (b) H<sub>2</sub> pressure (Reaction conditions: 0.228 g BPA (1.0 mmol), 0.05 g catalyst, 150 °C, 800 rpm agitation speed, 10 ml decane, and 1 h; (c) Solvent (Reaction conditions: 0.228 g BPA (1.0 mmol), 0.05 g catalyst, 3.0 MPa H<sub>2</sub>, 150 °C, 800 rpm agitation speed, 1 h. (d) Time (Reaction conditions: 0.228 g BPA (1.0 mmol), 0.05 g catalyst, 3.0 MPa H<sub>2</sub>, 150 °C, 800 rpm agitation speed, 10 ml decane. TON for BPA conversion was calculated by (mol<sub>BPA</sub> consumed/mol<sub>Ru</sub> metal). [Data comparison, including BPA conversion and product selectivity with respect to temperature, H<sub>2</sub> pressure, solvent, and time is given in Fig. S12].

depolymerization of plastic feedstocks and selectivity toward the desired product. Fig. 4c depicts the effect of solvent on BPA conversion, product yield, and TON, while the relationship between product selectivity and BPA conversion is displayed in Fig. S12c. Results suggest that the solvent played an important role in activating and poisoning the C-O and C-C bonds in BPA HDO. The site-specific inhibition and structure-activity relationship of BPA with solvent and catalyst were studied by Y. Wang et al. for selective Csp<sup>2</sup>-Csp<sup>3</sup> bond cleavage [53]. Methanol preserves the Csp<sup>2</sup>-O bond and promotes the Csp<sup>2</sup>-Csp<sup>3</sup> bond cleavage by poisoning the surface acidic sites of Nb<sub>2</sub>O<sub>5</sub>, and the products obtained were monocyclic oxygenates and oxygenates [53]. In the present study, the complete conversion of BPA (TON = 204) and 86.4% of Csp<sup>2</sup>-Csp<sup>3</sup> bond cleaved monocyclic oxygenates, mainly phenolics was obtained in methanol, which is in line with the conclusion obtained by Y. Wang et al. It is worth mentioning that the present catalytic system also worked for selective Csp<sup>2</sup>-Csp<sup>3</sup> cleavage by site-specific inhibition of catalyst and

attributed selective phenolics under mild reaction conditions. But in this work, the emphasis was to achieve complete hydrodeoxygenation of BPA/PC to produce jet fuel range hydrocarbons (especially P7). A 99.9% BPA conversion and 97.3% P7 yield were obtained in decane, while 93.8% BPA conversion and 70.2% P7 yield were obtained in water (Fig. S12c). The bond dissociation energy of Csp<sup>2</sup>-Csp<sup>3</sup> (370 kJ mol<sup>-1</sup>) [54] is lower due to the electron-donation effect of the two -CH<sub>3</sub> group, facilitating the cleavage of Csp<sup>2</sup>-Csp<sup>3</sup> bond through a reverse Friedel-Crafts reaction in water [55]. The highest P7 selectively was obtained in decane at 150 °C, 3.0 MPa H<sub>2</sub>, and 0.05 g of 1Ru0.5Ni/H-Beta (Ni/Ru = 0.5) catalyst for 1 mmol BPA.

It has been observed that the polarity of the solvent has a significant impact on the hydrogenation reaction mechanism, as demonstrated by the selectivity obtained for cycloalkanes and cycloalcohol in nonpolar and polar solvents, respectively. A recent study by Xia, H. et al., suggests that the solvent has a negligible effect on the reaction energy barriers. It



can significantly impact the hydration reaction of cyclohexanol. The polarity of the solvent hinders the adsorption of the substrate on the catalyst surface, resulting in the non-planar adsorption of cyclic alcohol. This, in turn, effectively inhibits the dehydration of cyclic alcohol to cycloalkanes [56]. In decane, the favorable adsorption of the aromatic ring would occur on the catalyst surface, and high conversion and selectivity were obtained, consistent with literature report [57,58]. A plot illustrating the relationship between the solvent's dielectric constant and the selectivity of the main product (P7) is presented (Fig. S13). As the dielectric constant increased from decane to methanol, the selectivity of P7 decreased. The polarity index is also plotted against P7 selectivity and found a good correlation (Fig. S13). However, the water did not follow such a trend. Since water forms hydrogen bonding with the substrates and catalysts, its influence differs from other solvents and thus does not follow the trend. Further, to find out the hydrogen solubility in different solvents, we extensively reviewed the literature related to hydrogen solubility in organic solvents. The hydrogen solubility for the solvents used in this study (decane, methanol, THF, and water) is not reported at the optimized temperature and pressure. However, Trinh T. K. H and co-workers use Henry's constant to investigate hydrogen solubility for different solvents, including alcohols, aldehydes, carboxylic acid, esters, ethers glycols, n-alkanes, and water [59]. The author stated that Henry's constant of the hydrogen increases with temperature, corresponding to a decrease in solubility. According to Trinh T. K. H and co-workers' investigation, oxygenated solvents have a higher Henry's constant than n-alkanes. The lower Henry's constant corresponds to higher hydrogen solubility. The higher hydrogen solubility in a non-polar solvent (decane) also contributes to higher HDO activity.

As the time increased from 0.25 h to 1 h, the P7 yield rose from 24% to 97%, the conversion of BPA increased from 40% to 99.9%, and a TON of BPA consumption increased from 81 to 204, respectively (Fig. 4d and Fig. S12d). Meanwhile, the P1-P3 yield also decreased (Fig. 4d). The complete conversion of BPA and the highest selectivity of P7 was obtained in 1 h (Fig. S12d), and no significant changes were observed in product selectivity when the time was extended. Thus, 1 h was the optimum time for this reaction.

The catalyst stability and reusability were investigated by several consecutive catalytic runs for 0.5 h over 1Ru0.5Ni/H-Beta catalyst. After each catalytic run, the catalyst was separated by centrifugation, washed with water: ethanol mixture (1:2), to remove the possibly adsorbed organic species, and dried at 80 °C overnight. Fig. S14a displayed excellent catalyst reusability for five catalytic runs. The conversion of BPA and P7 selectivity was nearly unchanged, which is a superior catalytic system to those previously reported (physically mixed catalytic systems). Data comparison of the first and fifth runs, including BPA conversion and product distribution after 0.5 h, is given in Fig. S14b. To investigate the change in the physicochemical properties that could occur in the spent catalyst, XRD, Py-IR, MP-AES, and XPS, were conducted (Fig. S16-18 and Table S4). All conducted characterization suggests that the active sites of the catalyst were not changed after five catalytic runs. Further, the metal leaching was conducted via a hot-filtration test. The catalyst was removed after 0.25 h in hot conditions (the BPA conversion was 39.4%), and the reaction mixture was again charged to proceed further without a catalyst. There was a minor increase in the BPA conversion (1.3%) even after 1 h of reaction time, confirming the heterogeneous catalytic process (Fig. S15).

### 3.3. Hydrodeoxygenation of polycarbonate (PC)

After evaluating all reaction parameters for BPA HDO, 1.0 mmol of BPA, 3.0 MPa H<sub>2</sub> pressure, and 1.0 h of reaction time were obtained to achieve the highest P7 yield with a complete conversion of BPA. Then, to fulfill the need for the actual PC waste upcycling, PC HDO was conducted under the optimized conditions of BPA HDO. The PC was obtained from a CD (purification procedure and physiochemical properties

are provided in supporting information Scheme S3, S4, & Table S1), directly introduced for direct HDO, offering low PC conversion and P7 yield under evaluated reaction conditions. Even after increasing the time, at 150 °C, no significant changes were observed for PC conversion and P7 yield, indicating the rigid polymeric structure of PC required a higher temperature to depolymerize polymer into monomer due to its high thermal stability, mechanical strength, and heat distortion temperature [60]. Therefore, after the extensive screening of various reaction parameters, relatively mild and efficient optimized conditions (180 °C and 10 h) were obtained for 1Ru0.5Ni/H-Beta and keeping all other parameters the same as optimized for BPA HDO. After the reaction, the catalyst and unreacted PC were separated from the reaction mixture to calculate the PC conversion and P7 selectivity (the equations S3-S4 were used for PC conversion, and P7 selectivity was provided in the supporting information) [21,22]. The reaction mixture was diluted with ethyl acetate and analyzed by GC and GC-MS, affording a nearly complete conversion of PC (99.9%), and 90.2% selectivity of P7 (Table 3, Entry 4).

Upon increasing the reaction temperature above 180 °C, the complete PC conversion was obtained within 7–8 h, and the lower selectivity of P7 was observed due to further cleavage of the C-C bond to lower density range chemicals (P3-P6), which was also observed in BPA HDO. The impact of solvent on the performance of PC HDO was evaluated by conducting experiments using THF and methanol, demonstrating a similar selectivity to that observed for BPA HDO. The reaction data for the influence of temperature and time are displayed in Fig. S19 a, b. The catalyst was also employed for the commercial polycarbonate purchased from Sigma-Aldrich (properties are provided in SI, Table S1) and afforded almost similar activity with complete PC conversion and 89.8% yield of P7 at the optimum conditions (0.2 g PC, 0.05 g catalyst, 3.0 MPa H<sub>2</sub> pressure, and 10 h) (Table 3, Entry 6). The catalytic reusability test was also conducted with PC at the optimized reaction conditions for 6 h. The results displayed no significant decrease in the PC conversion (4.9%), but a marginal reduction in P7 yield (13%) was observed (Fig. S20), suggesting that the catalyst was stable even after five catalytic runs. The coke formation on the catalyst was tested by TGA analysis (Fig. S21), which indicates that an unreacted coke adsorbed on the catalyst had no significant effect on catalytic activity. After removing the coke and activating the catalyst under H<sub>2</sub>/Ar, the catalyst regained its activity, suggesting the coke had physically enveloped the active sites responsible for a marginal decrease in P7 selectivity (Fig. S20).

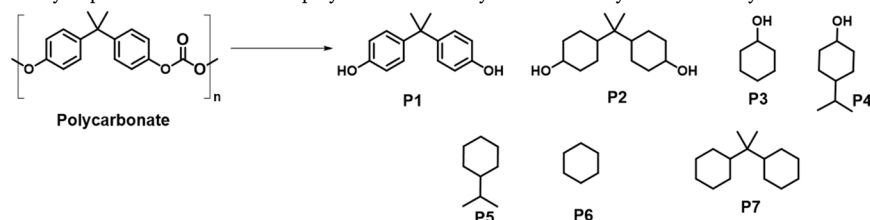
The catalytic process was scaled up to 2 g of PC waste. In this case, ~90% PC conversion and ~89% P7 selectivity were achieved under the optimized conditions. Such encouraging results suggest that further optimization will be needed based on the batch size. In state of the art, only one report exists that employed a combination of two catalysts (Rh/HY + HY) to catalyze this reaction and afforded ~99% PC conversion with ~87% P7 selectivity at 200 °C for 12 h. A single cheap catalyst 1Ru0.5Ni/H-Beta of this study afforded better P7 selectivity (90.2%) at a similar conversion level (~99%) but at relatively milder reaction conditions (180 °C for 10 h). The two-catalyst system reported in the prior art is difficult to separate and reactivate for the fresh cycle. In contrast, the present catalyst can be efficiently separated and recycled. A detailed structure-activity relationship is provided here, which was somewhat lacking in the literature.

### 3.4. Investigating and understanding the HDO mechanism

To shed light on the synergy between Ru and Ni and investigate the reaction mechanism for Ru/H-Beta and Ru-Ni/H-Beta catalysts, reaction kinetics were studied over 1Ru/H-Beta and 1Ru0.5Ni/H-Beta catalysts. To understand the pathway of HDO, different parameters such as BPA concentration, H<sub>2</sub> pressure, and temperature were evaluated for 0.5 h (Fig. S23). The stirring speed was optimized to 800 rpm to ensure the kinetic regime and avoid the gas-liquid mass transfer effect (Fig. S22). The kinetic study revealed that both catalysts show different adsorption

**Table 3**

Catalytic performance for HDO of polycarbonate over synthesized catalysts of this study.



No.	Catalyst	Conv. (%)	Product distribution (% Selectivity) <sup>b</sup>				
			P1	P2	P3-P4	P5-P6	P7
1.	H-Beta	12.8	24.1	-	-	-	-
2.	1Ni/H-Beta	34.3	11.6	-	-	-	-
3.	1Ru/H-Beta	42.2	6.6	1.6	0.6	16.3	72.0
4.	1Ru0.5Ni/H-Beta	99.9	-	-	0.8	7.8	90.2
5.	1Ru1Ni/H-Beta	99.9	-	-	-	24.3	75
6.	1Ru0.5Ni/H-Beta <sup>c</sup>	99.9	-	-	-	6.4	88.6
7.	1Ru0.5Ni/H-Beta <sup>d</sup>	90.6	-	-	-	8.2	89.4

<sup>a</sup>Reaction conditions: 0.2 g of PC (CD disk), 0.05 g of catalyst, 10 ml of decane, 3.0 MPa H<sub>2</sub>, stirred at 800 rpm, 180 °C, and 10 h. <sup>b</sup>Selectivity of P7 was calculated by desired product/total products \* 100. <sup>c</sup> Using commercial PC. <sup>d</sup>Gram scale reaction of PC.

properties and behave differently in the HDO of BPA. From XPS and H<sub>2</sub>-TPR results, it was found that the interaction between Ru and Ni led to a favourable electron transfer from Ni to Ru, resulting in a higher spin-up d-band centre value of surface atoms, which may exhibit a different adsorption property from the monometallic catalysts. In the case of 1Ru/H-Beta, the conversion of BPA decreased with an increase in BPA concentration (Fig. 5a). The order of reaction with respect to BPA concentration was calculated by plotting a graph of  $\ln$  (initial rate) vs  $\ln$  (BPA concentration). From the slope of the graph (Fig. 5b), the order of reaction was 0.90, which is close to 1st order with respect to BPA concentration. On the other hand, for 1Ru0.5Ni/H-Beta catalyst, the order of the reaction was 0.2, indicating that the reaction is close to zero order with respect to BPA concentration (Fig. 5h). The zero-order over 1Ru0.5Ni/H-Beta suggests effective adsorption of BPA on the bimetallic Ru-Ni alloy and quick transformation into P7. The first order over 1Ru/H-Beta implies the moderate activation of BPA on the Ru sites of the 1Ru/H-Beta catalyst [61]. Several theoretical studies have shown that the synergistic effect of two metals in bimetallic catalysts can form a metal-metal bond, resulting in changes in their electronic properties. These changes in electronic properties enhance the adsorption of phenolics and ultimately result in superior catalytic activity compared to monometallic catalysts [62,63]. The zero-order with respect to BPA concentration over 1Ru0.5Ni/H-Beta catalyst suggests that the Ru-Ni alloy sites were fully saturated with the BPA due to favorable adsorption, and once adsorbed, the reaction proceeds quickly to form the products, and a further increase in BPA concentration does not significantly impact on the reaction rate [64]. The effect of H<sub>2</sub> pressure on the kinetic was also investigated. It was observed that both catalysts apparently showed close to 1st-order dependence on hydrogen pressure, indicating no obvious effect on reaction rate with H<sub>2</sub> pressure by the addition of Ni metal [64]. Further, the activation energy for both catalysts was calculated by performing four sets of reactions at different temperatures. The lower activation energy in 1Ru0.5Ni/H-Beta (63.5 kJ mol<sup>-1</sup>) than 1Ru/H-Beta (84.7 kJ mol<sup>-1</sup>) confirmed that the reaction was more facile over 1Ru0.5Ni/H-Beta. Additionally, the activation enthalpy ( $\Delta H$ ) and free energy of activation ( $\Delta G$ ) for the HDO of BPA over 1Ru/H-Beta and 1Ru0.5Ni/H-Beta at 110 °C were determined using the Arrhenius plot [65]. The values of  $\Delta H$  and  $\Delta G$  were calculated using the equations  $\Delta H = E_a - RT \ln(N_A h k / RT)$ , respectively. Here, R is the gas constant (8.314 J mol<sup>-1</sup> K<sup>-1</sup>), T is the temperature in K, N<sub>A</sub> is Avogadro's number (6.02214076 × 10<sup>23</sup>), h is Planck's constant (6.62607015 × 10<sup>-34</sup> m<sup>2</sup> kg/s), and k is the rate constant. The calculated values of  $E_a$ ,  $\Delta H$ , and  $\Delta G$  were 84.7 kJ mol<sup>-1</sup>, 81.39 kJ mol<sup>-1</sup>, and 38.13 kJ mol<sup>-1</sup> for HDO of BPA over 1Ru/H-Beta,

and 63.5 kJ mol<sup>-1</sup>, 60.2 kJ mol<sup>-1</sup>, and 37.83 kJ mol<sup>-1</sup> for HDO of BPA over 1Ru0.5Ni/H-Beta, respectively.

The catalytic performance of the HDO reaction is influenced by the adsorption of BPA and hydrogen on active sites of the catalyst surface. The aromatic compound with the -OH group (Phenolic) has great potential to adsorb on zeolites (through bridging oxygen) due to the electron-donation effect of the phenolic -OH group and forms the phenolate ion species [66]. The Brønsted acid zeolites also have a great affinity for HDO of phenolic, so it is crucial to understand the interaction between the Brønsted acid sites and phenolic compounds. *p*-Cresol was used as a probe molecule for the DRIFT study to rationalize the interaction between surface acidity and phenolic substrate and the adsorption capacity of the catalysts. *p*-Cresol adsorbed DRIFT spectra were recorded at different temperatures (150 °C, 200 °C, and 250 °C) over different catalysts (Fig. S25 and S26).

*p*-Cresol shows FT-IR peaks at 1621 cm<sup>-1</sup>, 1605 cm<sup>-1</sup> and 1516 cm<sup>-1</sup>, corresponding to C<sub>Ar</sub>=C<sub>Ar</sub> stretching vibration of the benzene ring (Fig. 6 & Fig. S25). The peak at 1357 cm<sup>-1</sup> corresponds to  $\nu$  (C-O) vibration suggesting the dissociation of hydrogen from phenolic oxygen and forming a cresolate species and the phenolic oxygen atom covalently bonded to Lewis acid sites of the catalyst (Fig. S26a) [67]. The catalysts showed the substituted phenol (*p*-cresol) stretching vibration at 1617, 1596, 1526, 1506, and 1378 cm<sup>-1</sup>, corresponding to aromatic species (C<sub>Ar</sub>=C<sub>Ar</sub>) and the methyl group (C<sub>Ar</sub>-CH<sub>3</sub>) that were formed on the surface with a slight shift towards the lower wavenumber, indicating that the benzene ring adsorbed on the Ru-Ni alloy sites of the 1Ru0.5Ni/H-Beta catalyst (Fig. 6a) [68]. It was observed that the area under the curve of the band corresponding to C<sub>Ar</sub>=C<sub>Ar</sub> adsorption (1526 cm<sup>-1</sup> and 1506 cm<sup>-1</sup>) increased after alloying Ni with Ru and further increased with the increase of the Ni content and the redshift for the C<sub>Ar</sub>=C<sub>Ar</sub> stretching of the *p*-cresol demonstrates the efficient hydrogenation ability of bimetallic Ru-Ni catalysts (Fig. 6 & Fig. S25-S26). The trend indicates that the electronic properties of Ru-Ni alloy enhanced the adsorption capacity, mainly through the C<sub>Ar</sub>=C<sub>Ar</sub> bond, and the results are consistent with a kinetic conclusion and experimental results (Fig. 5 & 6). The DRIFT adsorption spectra revealed that the bimetallic Ru-Ni has a great potential for effective adsorption of the aromatic substrate and subsequent hydrogenation to cyclic hydrocarbon. Further, the role of Brønsted acid sites of H-Beta in HDO reaction was investigated by performing two control experiments with pyridine and 2, 6 tert-butyl pyridine (TBP) treated catalyst (passivation procedure is provided in supporting information) under identical reaction conditions (Fig. 6b). It is reported that the pyridine (d = 0.53 nm) is protonated by Brønsted acid sites and coordinates to Lewis acid sites of zeolite, while the

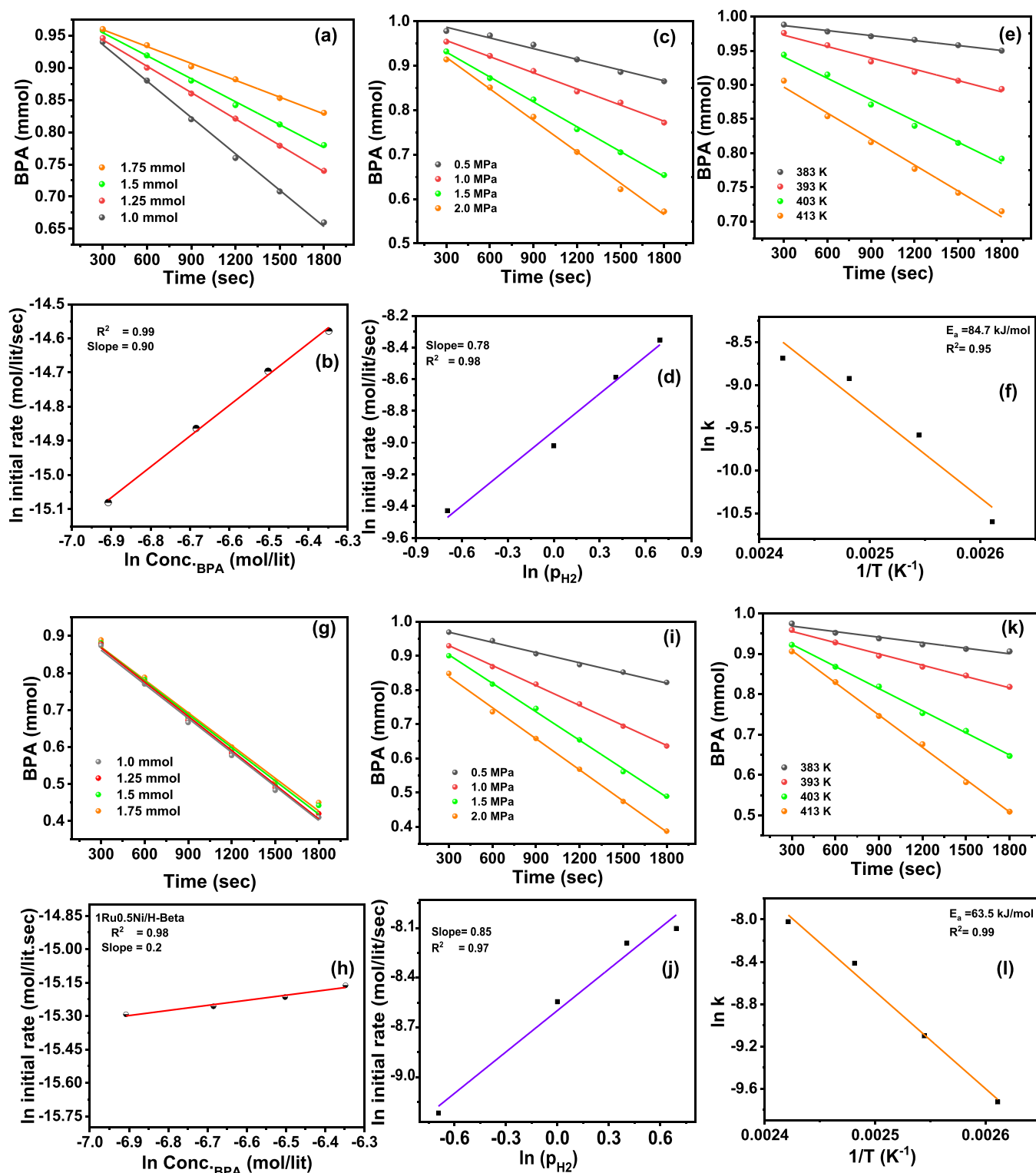


Fig. 5. BPA concentration as a function of time, reaction order, and apparent activation energies for HDO of BPA over 1Ru/H-Beta (a-f) and 1Ru0.5Ni/H-Beta (g-l). The kinetic experiment data comparison including BPA conversion and product selectivity with respect to time, is given in Fig. S23.

sterically hindered 2,6 (TBP) ( $d=1.05$  nm) can interact only with the Brønsted acid sites of the zeolite. Fig. 6b revealed that the catalyst passivated with pyridine showed only 16% conversion of BPA, indicating that pyridine poisoned all active sites of the catalyst, including both types of acid sites of H-Beta and the Ru-Ni alloy sites. In contrast, the reaction under 2,6 TPB passivated catalysts resulted in the complete conversion of BPA with the selective formation of cyclic alcohol,

suggesting that only surface Brønsted acid sites were affected by 2,6 TPB and not the Ru-Ni alloy sites. Overall, results indicate that the higher selectivity of cyclic alcohol and a significant decrease in the P7 selectivity in control experiments confirm the indispensable role of the surface Brønsted acid sites in promoting the dissociation of the C-O bond [69].

To gain more insight into the structure-activity relationship with Ru-

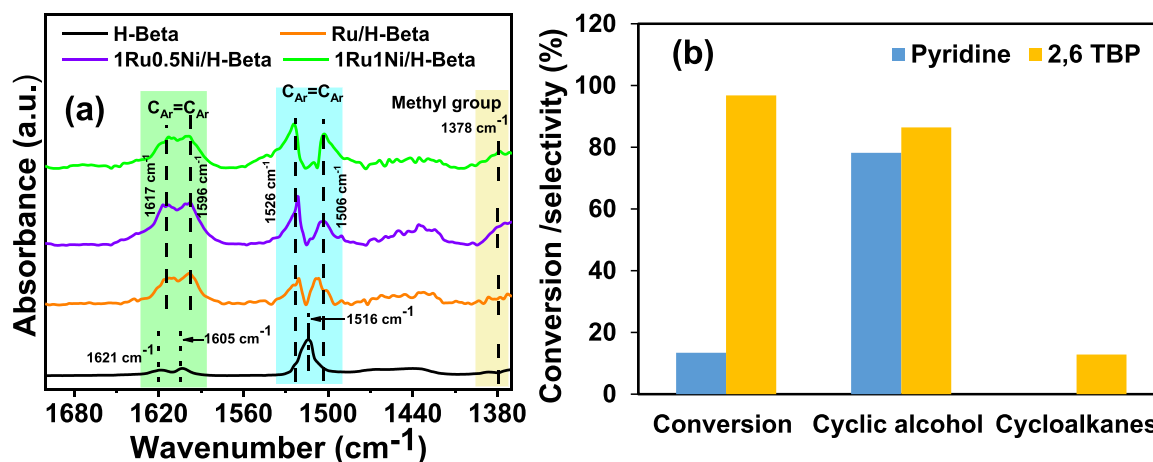


Fig. 6. *p*-Cresol adsorbed DRIFT spectra over catalysts at 200 °C (a); control experiments to investigate the role of acidic site (b), Reaction conditions: 0.228 g BPA (1.0 mmol), 0.05 g passivated 1Ru0.5Ni/H-Beta (pyridine/2,6 TBP), 3.0 MPa H<sub>2</sub>, 800 rpm agitation speed, 10 ml decane, 150 °C, and 1 h.

Ni alloy and acidic sites of H-Beta in HDO reaction, various substituted phenolic compounds, including diphenyl carbonate (DPC), which is a suitable model substrate having a similar structure to PC, were evaluated. All substrates were transformed to the corresponding cycloalkane with excellent TOFs and yield (Table 4). In Fig. 7a, the possible pathways for the depolymerization of polycarbonate (PC) to bisphenol A (BPA) via hydrolysis (due to the presence of moisture in the solvent, which was further confirmed by the addition of a small amount of water in the solvent) and hydrogenolysis (under hydrogen atmosphere) are presented. The depolymerization pathway of PC was investigated and observed that hydrogenolysis is the predominant pathway leading to BPA. Two separate experiments were performed with and without hydrogen, respectively. Additionally, upon the addition of water into the reaction mixture, no significant difference in the activity was observed in PC conversion, indicating the hydrogenolysis was the predominant pathway (Fig. 7b). Further, the hydrogenolysis pathways of PC or DPC were explored, and two potential pathways were identified: one involving the cleavage of the bond between oxygen and benzene to form aromatics and the other involving the cleavage of the bond between the carbonyl carbon and phenolic oxygen to form phenolic compounds (Fig. 7c). Two sets of reactions were performed to confirm the major hydrogenolysis pathway (Fig. 7d). The extent of conversion for diphenylmethane (DPM) to corresponding cycloalkane was lower than that of bisphenol F (BPF) (Fig. 7d), indicating that the phenolic oxygen plays a crucial role in the adsorption and subsequent hydrogenation to the targeted compound. Overall, results suggest that PC initially depolymerized through hydrogenolysis, involving the cleavage of the bond between the phenolic oxygen and a carbonyl group, leading to the formation of BPA. Subsequently, BPA is converted to cyclic hydrocarbons. Moreover, the generation of CH<sub>4</sub> was observed during the HDO of PC, which is most likely produced by the methanation of CO (Fig. S27). Nonetheless, the absence of a distinct CO peak in the gaseous mixture suggests that the methanation reaction proceeded rapidly.

### 3.5. Reaction mechanism for PC HDO

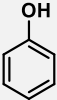
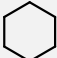
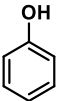
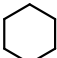
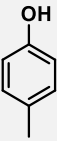
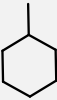

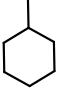
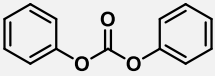
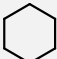
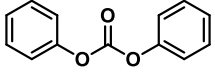
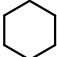
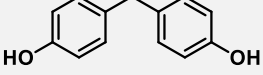
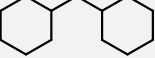
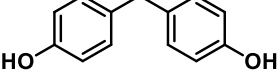
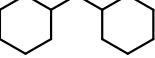
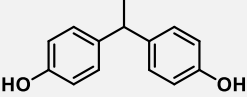
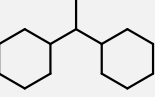
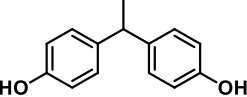
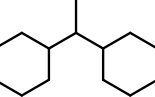
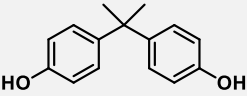
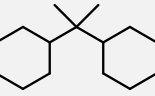
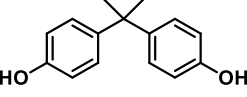
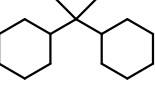
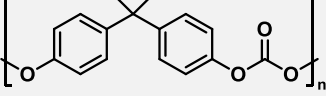
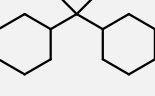
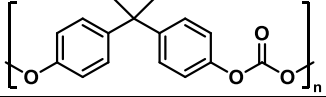
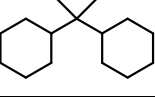
Based on the control experiments, it is suggested that PC can be cleaved by the hydrogenolysis of the carbonyl carbon and phenolic oxygen and forms the BPA (supported by control experiments, Fig. 7a-d). Further in the BPA HDO, oxygen removal from BPA is mainly through the HDO step over a Ru-based bi-functional bimetallic catalyst. Based on the activity data, products observed during the HDO, kinetic analysis, and DRIFT results, a reaction mechanism is proposed. BPA adsorbed on the catalyst through the C<sub>Ar</sub>=C<sub>Ar</sub> bond (investigated by kinetic and DRIFT experiment), and the dissociation of H<sub>2</sub> occurred on the Ru sites

of the catalyst (confirmed by H<sub>2</sub>-TPD). The dissociative adsorbed hydrogen is transferred to the adsorbed aromatic ring through the Ru-Ni alloy-support interface, and the subsequent ring hydrogenation of BPA leads to the formation of 4, 4'-(propane-2, 2-dial) bis (cyclohexan-1-ol) (P2) by consecutive ring hydrogenation (Scheme 2, route 1a). In contrast, the monometallic Ru/H-Beta behaves in a quite different mechanism for product P7. Especially, Ru/H-Beta offers the single-ring hydrogenation of BPA followed by cleavage of the Csp<sup>3</sup>–OH bond, leading to the formation of P1 (observed during the reaction) and further the subsequent ring hydrogenation and Csp<sup>3</sup>–OH bond cleavage forms product P7 (Scheme 2, route 1b). The surface Brønsted acid sites catalyzed the cleavage of the Csp<sup>3</sup>–OH bond by hydrogenolysis of alcohol, which was proved by selective acid site poisoning experiments and also in line with the literature [56,63]. The surface Brønsted acidic site with Ru-Ni alloy phases helps to cleave the Csp<sup>3</sup>–OH bond, followed by the formation of cyclic hydrocarbon (P7) (confirmed by poisoning experiments, Fig. 6). The hydrogenation of the aromatic ring and subsequent hydrogenolysis of cyclic alcohol involved in the BPA HDO. The reaction order for hydrogenation and hydrogenolysis was calculated using model compounds such as phenol and cyclohexanol, respectively. The order of reaction for hydrogenation was calculated by plotting a graph of ln (initial rate) vs ln (phenol concentration). From the slope of the graph, the order of reaction was 0.23, which is close to zero order. On the other hand, the order of reaction for hydrogenolysis was found 0.8, indicating that the reaction is close to 1st order with respect to cyclohexanol (Fig. S24). In addition, products P3-P6 can be produced by cleavage of the Csp<sup>2</sup>-Csp<sup>3</sup> bond through a reverse Friedel–Crafts reaction of BPA to phenol, and it can be further converted to product P3-P6 through the ring hydrogenation and Csp<sup>3</sup>–OH bond cleavage (Scheme 2 route 3). The unconventional route 2 is quite hard to happen due to the high activation barrier of the C<sub>Ar</sub>–OH bond [54]. Moreover, the C<sub>Ar</sub>–OH bond cleave products/intermediate was not observed during the HDO of PC/BPA. In addition, the diphenylmethane was not effectively converted into a targeted product under identical reaction conditions (Fig. 7). Thus, it can be concluded that route 2 was kinetically disfavoured over the 1Ru0.5Ni/H-Beta catalyst under identical reaction conditions. Finally, considering all the investigated results and evidence, the mechanistic pathway for HDO of PC to P7 is proposed (Scheme 3). PC is depolymerized through hydrogenolysis, involving the cleavage of the bond between the phenolic oxygen and a carbonyl group, leading to the formation of BPA. The subsequent ring hydrogenation of BPA leads to the formation of 4, 4'-(propane-2, 2-dial) bis (cyclohexan-1-ol) (P2) by consecutive ring hydrogenation, followed by hydrogenolysis to produce P7 as a selective product.

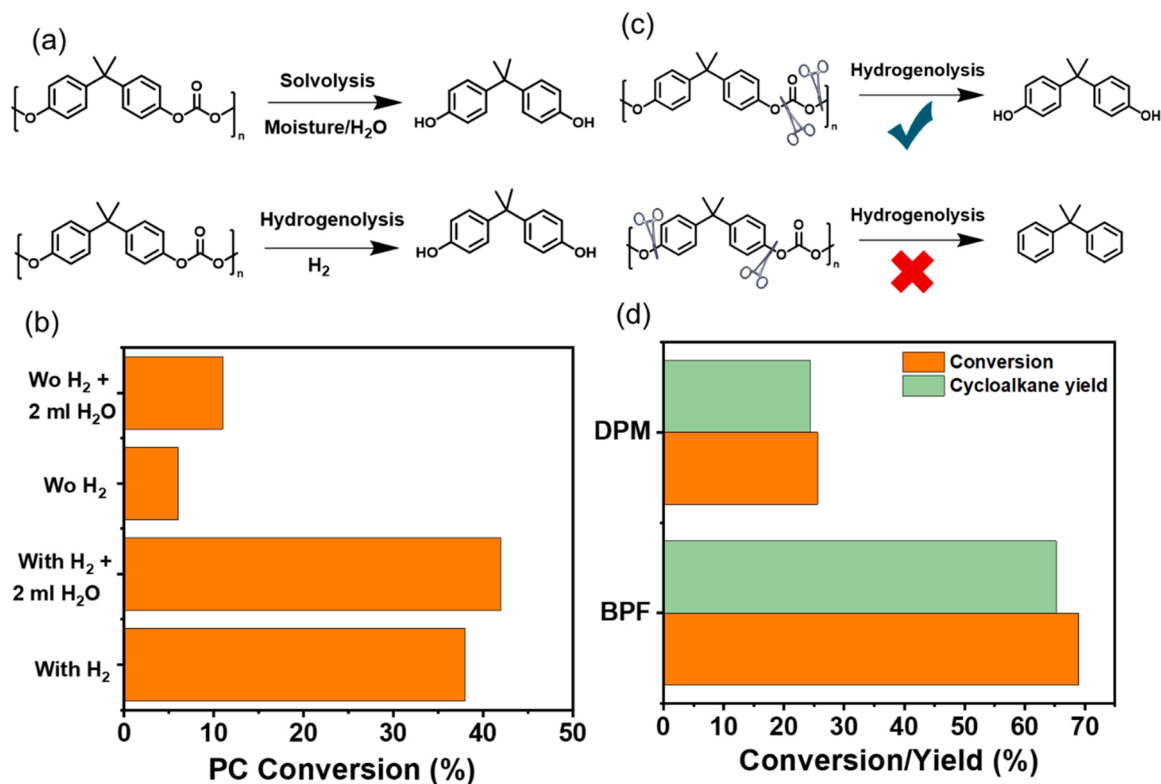


**Table 4**

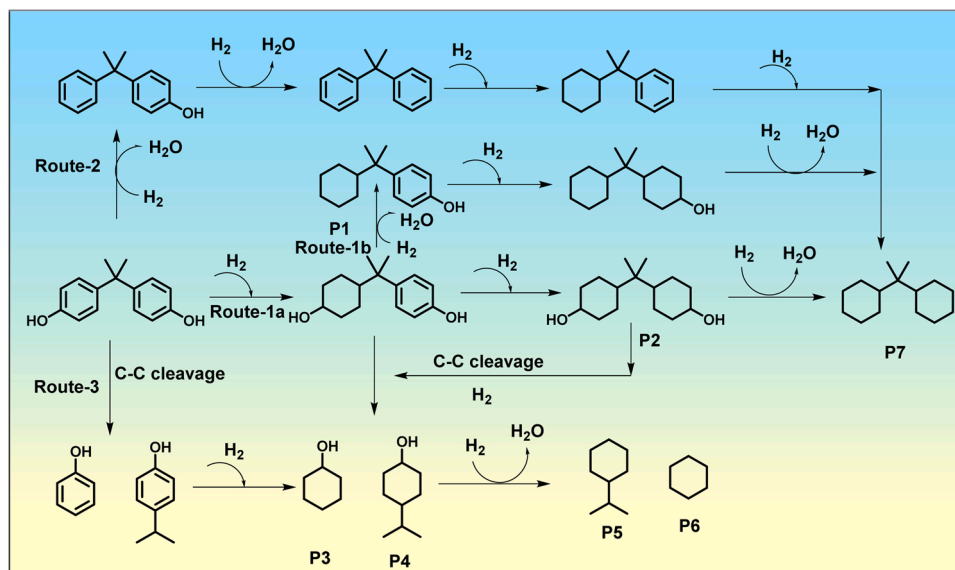
HDO of various mono and bicyclic phenolic substrate over 1Ru/H-Beta and 1Ru0.5Ni/H-Beta.

Substrate	Catalyst	Conversion (%)	Main product	Yield (%)	TOFs <sup>b</sup>
	1Ru/H-Beta	73.8		71.4	145
	1Ru0.5Ni/H-Beta	99.9		99.9	203
	1Ru/H-Beta	70.2		68.8	140
	1Ru0.5Ni/H-Beta	99.9		99.9	203
	1Ru/H-Beta	70.1		64.8	132
	1Ru0.5Ni/H-Beta	92.1		89.7	183
	1Ru/H-Beta	62.8		62.0	126
	1Ru0.5Ni/H-Beta	99.9		99.1	202
	1Ru/H-Beta	64.1		62.4	127
	1Ru0.5Ni/H-Beta	99.9		98.0	200
	1Ru/H-Beta	63.4		58.9	120
	1Ru0.5Ni/H-Beta	99.9		97.2	198.3
	1Ru/H-Beta <sup>a</sup>	42.2		36.9	8.6
	1Ru0.5Ni/H-Beta <sup>a</sup>	99.9		90.2	18.4

Reaction conditions: Substrate (1.0 mmol), 0.05 g catalyst, 3.0 MPa H<sub>2</sub>, 800 rpm agitation speed, decane, 150 °C temperature, and 1 h. <sup>a</sup> Reaction condition: PC (0.2 g), 0.05 g catalyst, 3.0 MPa H<sub>2</sub>, 800 rpm agitation speed, decane, 180 °C, and 10 h. <sup>b</sup> TOFs were calculated by (mol<sub>main product</sub> formed/mol<sub>Ru metal</sub>/1 h).



**Fig. 7.** Possible pathways for depolymerization of PC (a); Performance of catalytic reaction with and without H<sub>2</sub> and water (b). Reaction conditions: 0.2 g of PC, 0.05 g of catalyst, 10 ml of decane, 800 rpm agitation speed, 180 °C, and 4 h; Possible hydrogenolysis pathway for PC (c). Control reactions were performed using bisphenol F (BPF) and diphenylmethane (DPF) (d). Reaction conditions: 0.20 g of substrate, 0.05 g of catalyst, 10 ml of decane, 3.0 MPa H<sub>2</sub>, 800 rpm agitation speed, 150 °C, and 0.5 h.

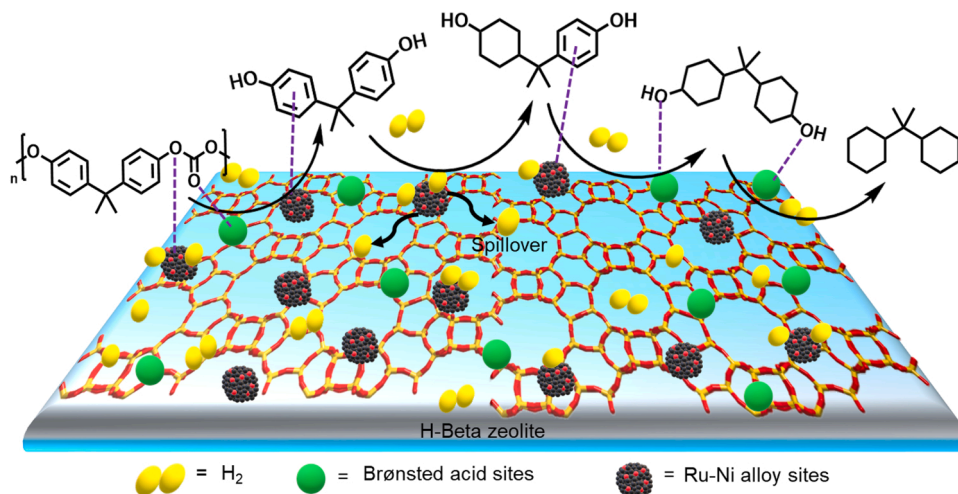


**Scheme 2.** Possible pathways for BPA HDO.

#### 4. Conclusions

In summary, the bi-functional bi-metallic alloy of Ru and Ni metal-supported H-Beta was prepared for the HDO of BPA and polycarbonate plastic waste to jet fuel chemicals. In-depth characterization confirmed strong interaction between Ru and Ni forming an alloy over the H-Beta zeolite and was subsequently proven to be the active site for the BPA/polycarbonate plastic waste transformation. The selectivity of

the target jet fuel depended on the weight ratio of Ru and Ni. A volcano curve with Ni/Ru weight ratio between 0 and 1.5 was presented to show that the Ni/Ru ratio of 0.5 was the best to achieve the high selectivity for jet fuel. An optimum Ni content promoted the high dispersion of Ru-Ni alloy, and it functioned as a preferential site for substrate adsorption. The Ru site facilitated the dissociative H<sub>2</sub> activation and hydrogenation of the aromatic ring. Site-specific poisoning experiments revealed that the surface Brønsted acid sites promoted the dissociation of the C–O



**Scheme 3.** Proposed reaction mechanism for HDO of PC to P7 over 1Ru0.5Ni/H-Beta catalyst.

bond. The polarity of the solvent had a decisive influence on the HDO reaction mechanism, which affected the adsorption of BPA on the Ru-Ni alloy and acid sites of the Ru-Ni/H-Beta catalyst. A scaleup and recyclable catalytic protocol with detailed structure-activity discussed in this study could potentially broaden the scope of possible end products from waste feedstock, thereby providing an expanded avenue for plastic conversion and biomass valorization.

#### CRediT authorship contribution statement

**Arjun K. Manal:** Conceptualization, all experimental work including the majority of characterizations, manuscript draft preparation. **Ganapati V. Shanbhag:** TPR and TPD investigations. **Rajendra Srivastava:** Conceptualization, Supervision, Writing – review & editing.

#### Declaration of Competing Interest

The authors declare that they have no known competing financial interests or personal relationships that could have appeared to influence the work reported in this paper.

#### Data Availability

Data will be made available on request.

#### Acknowledgments

AKM is grateful to Ministry of Education, Government of India for PMRF fellowship (PMRF-ID, 2902500). RS thanks the research and Innovation award from IIT Ropar. The authors thank SAIF IIT Bombay for the TEM analysis and IIT Mandi for the XPS analysis.

#### Appendix A. Supporting information

Supplementary data associated with this article can be found in the online version at [doi:10.1016/j.apcatb.2023.123021](https://doi.org/10.1016/j.apcatb.2023.123021).

#### References

- [1] H. Li, H.A. Aguirre-Villegas, R.D. Allen, X. Bai, C.H. Benson, G.T. Beckham, S. L. Bradshaw, J.L. Brown, R.C. Brown, V.S. Cecon, J.B. Curley, G.W. Curtzwiler, S. Dong, S. Gaddameedi, J.E. García, I. Hermans, M.S. Kim, J. Ma, L.O. Mark, M. Mavrikakis, O.O. Olafasakin, T.A. Osswald, K.G. Papanikolaou, H. Radhakrishnan, M.A. Sanchez Castillo, K.L. Sánchez-Rivera, K.N. Tumu, R. C. Van Lehn, K.L. Vorst, M.M. Wright, J. Wu, V.M. Zavala, P. Zhou, G.W. Huber, Expanding plastics recycling technologies: chemical aspects, technology status, and challenges, *Green. Chem.* 24 (2022) 8899–9002, <https://doi.org/10.1039/D2GC02588D>.
- [2] Z. Dong, W. Chen, K. Xu, Y. Liu, J. Wu, F. Zhang, Understanding the structure-activity relationships in catalytic conversion of polyolefin plastics by zeolite-based catalysts: a critical review, *ACS Catal.* 12 (2022) 14882–14901, <https://doi.org/10.1021/acscatal.2c04915>.
- [3] K. Lee, Y. Jing, Y. Wang, N. Yan, A unified view on catalytic conversion of biomass and waste plastics, *Nat. Rev. Chem.* 6 (2022) 635–652, <https://doi.org/10.1038/s41570-022-00411-8>.
- [4] C. Wang, H. Han, Y. Wu, D. Astruc, Nanocatalyzed upcycling of the plastic wastes for a circular economy, *Coord. Chem. Rev.* 458 (2022), 214422, <https://doi.org/10.1016/j.ccr.2022.214422>.
- [5] I. Vollmer, M.J.F. Jenks, M.C.P. Roelands, R.J. White, T. Harmelen, P. Wild, G. P. Laan, F. Meirer, J.T.F. Keurentjes, B.M. Weckhuysen, Beyond Mechanical Recycling: Giving New Life to Plastic Waste, *Angew. Chem., Int. Ed. Engl.* 59 (2020) 15402–15423, <https://doi.org/10.1002/anie.201915651>.
- [6] E. Barnard, J.J. Rubio Arias, W. Thielemans, Chemolytic depolymerisation of PET: a review, *Green. Chem.* 23 (2021) 3765–3789, <https://doi.org/10.1039/D1GC00887K>.
- [7] C.-H. Wu, L.-Y. Chen, R.-J. Jeng, S.A. Dai, 100% atom-economy efficiency of recycling polycarbonate into versatile intermediates, *ACS Sustain. Chem. Eng.* 6 (2018) 8964–8975, <https://doi.org/10.1021/acssuschemeng.8b01326>.
- [8] T. Do, E.R. Baral, J.G. Kim, Chemical recycling of poly(bisphenol A carbonate): 1,5,7-Triazabicyclo[4.4.0]-dec-5-ene catalyzed alcoholysis for highly efficient bisphenol A and organic carbonate recovery, *Polym. (Guildf.)* 143 (2018) 106–114, <https://doi.org/10.1016/j.polymer.2018.04.015>.
- [9] T.-W. Jiang, K.S.K. Reddy, Y.-C. Chen, M.-W. Wang, H.-C. Chang, M.M. Abu-Omar, C.-H. Lin, Recycling waste polycarbonate to bisphenol a-based oligoesters as epoxy-curing agents, and degrading epoxy thermosets and carbon fiber composites into useful chemicals, *ACS Sustain. Chem. Eng.* 10 (2022) 2429–2440, <https://doi.org/10.1021/acssuschemeng.1c07247>.
- [10] A.A. Adeyi, B.A. Babalola, Bisphenol-A (BPA) in foods commonly consumed in southwest Nigeria and its human health risk, *Sci. Rep.* 9 (2019) 17458, <https://doi.org/10.1038/s41598-019-53790-2>.
- [11] T. Vasiljevic, T. Harner, Bisphenol A and its analogues in outdoor and indoor air: properties, sources and global levels, *Sci. Total Environ.* 789 (2021), 148013, <https://doi.org/10.1016/j.scitotenv.2021.148013>.
- [12] M.S. Muhamad, M.R. Salim, W.J. Lau, Z. Yusop, A review on bisphenol A occurrences, health effects and treatment process via membrane technology for drinking water, *Environ. Sci. Pollut. Res.* 23 (2016) 11549–11567, <https://doi.org/10.1007/s11356-016-6357-2>.
- [13] *Polycarbonate Market Size, Share & Trends Analysis Report By Application (Automotive & Transportation, Construction, Packaging, Consumer Goods, Others), By Region, And Segment Forecasts, 2022 - 2030*, (2020).
- [14] X. Wei, J. Yu, J. Du, L. Sun, New insights into the pyrolysis behavior of polycarbonates: a study based on DFT and ReaxFF-MD simulation under nonisothermal and isothermal conditions, *Energy Fuels* 35 (2021) 5026–5038, <https://doi.org/10.1021/acs.energyfuels.1c00133>.
- [15] Y. Jing, Y. Wang, S. Furukawa, J. Xia, C. Sun, M.J. Hülsey, H. Wang, Y. Guo, X. Liu, N. Yan, Towards the circular economy: converting aromatic plastic waste back to arenes over a Ru/Nb<sub>2</sub>O<sub>5</sub> catalyst, *Angew. Chem., Int. Ed. Engl.* 60 (2021) 5527–5535, <https://doi.org/10.1002/anie.202011063>.
- [16] H. Jin, B. Bai, W. Wei, Y. Chen, Z. Ge, J. Shi, Hydrothermal liquefaction of polycarbonate (PC) plastics in sub-/supercritical water and reaction pathway exploration, *ACS Sustain. Chem. Eng.* 8 (2020) 7039–7050, <https://doi.org/10.1021/acssuschemeng.0c00700>.
- [17] W. Huang, H. Wang, X. Zhu, D. Yang, S. Yu, F. Liu, X. Song, Highly efficient application of Mg/Al layered double oxides catalysts in the methanolysis of

- polycarbonate, *Appl. Clay Sci.* 202 (2021), 105986, <https://doi.org/10.1016/j.clay.2021.105986>.
- [18] F. Iannone, M. Casiello, A. Monopoli, P. Cotugno, M.C. Sportelli, R.A. Picca, N. Cioffi, M.M. Dell'Anna, A. Nacci, Ionic liquids/ZnO nanoparticles as recyclable catalyst for polycarbonate depolymerization, *J. Mol. Catal. A Chem.* 426 (2017) 107–116, <https://doi.org/10.1016/j.molcata.2016.11.006>.
- [19] M. Taguchi, Y. Ishikawa, S. Kataoka, T. Naka, T. Funazukuri, CeO<sub>2</sub> nanocatalysts for the chemical recycling of polycarbonate, *Catal. Commun.* 84 (2016) 93–97, <https://doi.org/10.1016/j.catcom.2016.06.009>.
- [20] D. Kim, B. Kim, Y. Cho, M. Han, B.-S. Kim, Kinetics of polycarbonate glycolysis in ethylene glycol, *Ind. Eng. Chem. Res.* 48 (2009) 685–691, <https://doi.org/10.1021/ie8010947>.
- [21] H. Tang, Y. Hu, G. Li, A. Wang, G. Xu, C. Yu, X. Wang, T. Zhang, N. Li, Synthesis of jet fuel range high-density polycycloalkanes with polycarbonate waste, *Green. Chem.* 21 (2019) 3789–3795, <https://doi.org/10.1039/C9GC01627A>.
- [22] L. Wang, G. Li, Y. Cong, A. Wang, X. Wang, T. Zhang, N. Li, Direct synthesis of a jet fuel range cycloalkane by the aqueous phase hydrodeoxygenation of polycarbonate, *Green. Chem.* 23 (2021) 3693–3699, <https://doi.org/10.1039/D1GC00353D>.
- [23] P. Sudarsanam, E. Peeters, E.V. Makshina, V.I. Parvulescu, B.F. Sels, Advances in porous and nanoscale catalysts for viable biomass conversion, *Chem. Soc. Rev.* 48 (2019) 2366–2421, <https://doi.org/10.1039/C8CS00452H>.
- [24] C. Zhang, F. Wang, Catalytic lignin depolymerization to aromatic chemicals, *Acc. Chem. Res.* 53 (2020) 470–484, <https://doi.org/10.1021/acs.accounts.9b00573>.
- [25] C. Michel, P. Gallezot, Why is ruthenium an efficient catalyst for the aqueous-phase hydrogenation of biosourced carbonyl compounds, *ACS Catal.* 5 (2015) 4130–4132, <https://doi.org/10.1021/acscatal.5b00707>.
- [26] W. Yu, M.D. Porosoff, J.G. Chen, Review of Pt-based bimetallic catalysis: from model surfaces to supported catalysts, *Chem. Rev.* 112 (2012) 5780–5817, <https://doi.org/10.1021/cr300096b>.
- [27] M. Martínez-Klimov, P. Mäki-Arvela, A. Çiftçi, N. Kumar, K. Eränen, M. Peurla, E.J. M. Hensen, D. Yu. Murzin, Bifunctional Pt–Re catalysts in hydrodeoxygenation of isoeugenol as a model compound for renewable jet fuel production, *ACS Eng. Au* 2 (2022) 436–449, <https://doi.org/10.1021/acseengineeringau.2c00015>.
- [28] X. Du, X. Lei, L. Zhou, Y. Peng, Y. Zeng, H. Yang, D. Li, C. Hu, H. Garcia, Bimetallic Ni and Mo nitride as an efficient catalyst for hydrodeoxygenation of palmitic acid, *ACS Catal.* 12 (2022) 4333–4343, <https://doi.org/10.1021/acscatal.1c05847>.
- [29] H. Wang, H. Ruan, M. Feng, Y. Qin, H. Job, L. Luo, C. Wang, M.H. Engelhard, E. Kuhn, X. Chen, M.P. Tucker, B. Yang, One-pot process for hydrodeoxygenation of lignin to alkanes using Ru-based bimetallic and bifunctional catalysts supported on zeolite Y, *ChemSusChem* 10 (2017) 1846–1856, <https://doi.org/10.1002/cssc.201700160>.
- [30] Z. Luo, Z. Zheng, L. Li, Y.-T. Cui, C. Zhao, Bimetallic Ru–Ni catalyzed aqueous-phase guaiacol hydrogenolysis at low H<sub>2</sub> pressures, *ACS Catal.* 7 (2017) 8304–8313, <https://doi.org/10.1021/acscatal.7b02317>.
- [31] S. Salakum, T. Yutthalekha, S. Shetsiri, T. Witoon, C. Wattanakit, Bifunctional and bimetallic Pt–Ru/HZSM-5 nanoparticles for the mild hydrodeoxygenation of lignin-derived 4-propylphenol, *ACS Appl. Nano Mater.* 2 (2019) 1053–1062, <https://doi.org/10.1021/acsnanm.8b02324>.
- [32] N. Ji, S. Cheng, Z. Jia, H. Li, P. Ri, S. Wang, X. Diao, Fabricating bifunctional Co–Al<sub>2</sub>O<sub>3</sub> @USY catalyst via in-situ growth method for mild hydrodeoxygenation of lignin to naphthenes, *ChemCatChem* 14 (2022), <https://doi.org/10.1002/cctc.202200274>.
- [33] F. Su, L. Lv, F.Y. Lee, T. Liu, A.I. Cooper, X.S. Zhao, Thermally reduced ruthenium nanoparticles as a highly active heterogeneous catalyst for hydrogenation of monoaromatics, *J. Am. Chem. Soc.* 129 (2007) 14213–14223, <https://doi.org/10.1021/ja072697v>.
- [34] A. Li, C. Huang, C.-W. Luo, W.-J. Yi, Z.-S. Chao, High-efficiency catalytic performance over mesoporous Ni/beta zeolite for the synthesis of quinoline from glycerol and aniline, *RSC Adv.* 7 (2017) 9551–9561, <https://doi.org/10.1039/C6RA26736J>.
- [35] Y. Zhao, W. Ke, J. Shao, F. Zheng, H. Liu, L. Shi, Rational design of multisite trielement Ru–Ni–Fe alloy nanocatalysts with efficient and durable catalytic hydrogenation performances, *ACS Appl. Mater. Interfaces* 11 (2019) 41204–41214, <https://doi.org/10.1021/acsaami.9b10398>.
- [36] J. Yang, Q. Shao, B. Huang, M. Sun, X. Huang, pH-universal water splitting catalyst: Ru–Ni nanosheet assemblies, *IScience* 11 (2019) 492–504, <https://doi.org/10.1016/j.isci.2019.01.004>.
- [37] A. Kumar, R. Bal, R. Srivastava, Modulation of Ru and Cu nanoparticle contents over CuAlPO-5 for synergistic enhancement in the selective reduction and oxidation of biomass-derived furan based alcohols and carbonyls, *Catal. Sci. Technol.* 11 (2021) 4133–4148, <https://doi.org/10.1039/D1CY00593F>.
- [38] G.T. Jaya, R. Insyani, J. Park, A.F. Barus, M.G. Sibi, V. Ranaware, D. Verma, J. Kim, One-pot conversion of lignocellulosic biomass to ketones and aromatics over a multifunctional Cu–Ru/ZSM-5 catalyst, *Appl. Catal. B: Environ.* 312 (2022), 121368, <https://doi.org/10.1016/j.apcatb.2022.121368>.
- [39] L. Fang, Z. Yan, J. Wu, A. Bugaev, C. Lamberti, M. Pera-Titus, Highly selective Ru/HBEA catalyst for the direct amination of fatty alcohols with ammonia, *Appl. Catal. B* 286 (2021), 119942, <https://doi.org/10.1016/j.apcatb.2021.119942>.
- [40] K. Mori, K. Miyawaki, H. Yamashita, Ru and Ru–Ni nanoparticles on TiO<sub>2</sub> support as extremely active catalysts for hydrogen production from ammonia–borane, *ACS Catal.* 6 (2016) 3128–3135, <https://doi.org/10.1021/acscatal.6b00715>.
- [41] G. Chen, S. Desinan, R. Rosei, F. Rosei, D. Ma, Synthesis of Ni–Ru alloy nanoparticles and their high catalytic activity in dehydrogenation of ammonia borane, *Chem. Eur. J.* 18 (2012) 7925–7930, <https://doi.org/10.1002/chem.201200292>.
- [42] R. Prins, Hydrogen spillover. Facts and fiction, *Chem. Rev.* 112 (2012) 2714–2738, <https://doi.org/10.1021/cr200346z>.
- [43] D. Kubická, N. Kumar, T. Venäläinen, H. Karhu, I. Kubičková, H. Österholm, D. Yu. Murzin, Metal–support interactions in zeolite-supported noble metals: influence of metal crystallites on the support acidity, *J. Phys. Chem. B* 110 (2006) 4937–4946, <https://doi.org/10.1021/jp055754k>.
- [44] Y. Geng, H. Li, Hydrogen spillover-enhanced heterogeneously catalyzed hydrodeoxygenation for biomass upgrading, *ChemSusChem* 15 (2022), <https://doi.org/10.1002/cssc.202102495>.
- [45] A.K. Manal, R. Srivastava, Zr–KIT-6 catalyzed renewable synthesis of N-aryl pyrroles for producing bioactive synthetic compounds, *Appl. Catal. A: Gen.* 650 (2023), 119018, <https://doi.org/10.1016/j.apcata.2022.119018>.
- [46] A.K. Manal, J.H. Advani, R. Srivastava, Bifunctional acid-base zirconium phosphonate for catalytic transfer hydrogenation of levulinic acid and cascade transformation of furfural to biofuel molecules, *ChemCatChem* 14 (2022), <https://doi.org/10.1002/cctc.202200576>.
- [47] L. Dong, L. Lin, X. Han, X. Si, X. Liu, Y. Guo, F. Lu, S. Rudić, S.F. Parker, S. Yang, Y. Wang, Breaking the limit of lignin monomer production via cleavage of interunit carbon–carbon linkages, *Chem* 5 (2019) 1521–1536, <https://doi.org/10.1016/j.chempr.2019.03.007>.
- [48] J. Zhang, J. Teo, X. Chen, H. Asakura, T. Tanaka, K. Teramura, N. Yan, A series of NiM (M = Ru, Rh, and Pd) bimetallic catalysts for effective lignin hydrogenolysis in water, *ACS Catal.* 4 (2014) 1574–1583, <https://doi.org/10.1021/cs401199f>.
- [49] R. Shu, R. Li, Y. Liu, C. Wang, P.-F. Liu, Y. Chen, Enhanced adsorption properties of bimetallic RuCo catalyst for the hydrodeoxygenation of phenolic compounds and raw lignin-oil, *Chem. Eng. Sci.* 227 (2020), 115920, <https://doi.org/10.1016/j.ces.2020.115920>.
- [50] L. Li, L. Dong, X. Liu, Y. Guo, Y. Wang, Selective production of ethylbenzene from lignin oil over FeOx modified Ru/Nb<sub>2</sub>O<sub>5</sub> catalyst, *Appl. Catal. B* 260 (2020), 118143, <https://doi.org/10.1016/j.apcatb.2019.118143>.
- [51] C. Crisafulli, S. Scirè, R. Maggiore, S. Minicò, S. Galvagno, CO<sub>2</sub> reforming of methane over Ni–Ru and Ni–Pd bimetallic catalysts, *Catal. Lett.* 59 (1999) 21–26, <https://doi.org/10.1023/A:1019031412713>.
- [52] S. Kumagai, M. Asakawa, T. Kameda, Y. Saito, A. Watanabe, C. Watanabe, N. Teramae, T. Yoshioka, Selective phenol recovery via simultaneous hydrogenation/dealkylation of isopropyl- and isopropenyl-phenols employing an H<sub>2</sub> generator combined with tandem micro-reactor GC/MS, *Sci. Rep.* 8 (2018) 13994, <https://doi.org/10.1038/s41598-018-32269-6>.
- [53] Y. Jing, M. Shakouri, X. Liu, Y. Hu, Y. Guo, Y. Wang, Breaking C–C bonds and preserving C–O bonds in aromatic plastics and lignin via a reversing bond energy cleavage strategy, *ACS Catal.* 12 (2022) 10690–10699, <https://doi.org/10.1021/acscatal.2c02924>.
- [54] K. Lee, Y. Jing, Y. Wang, N. Yan, A unified view on catalytic conversion of biomass and waste plastics, *Nat. Rev. Chem.* 6 (2022) 635–652, <https://doi.org/10.1038/s41570-022-00411-8>.
- [55] S.E. Hunter, P.E. Savage, Kinetics and mechanism of p-isopropenylphenol synthesis via hydrothermal cleavage of bisphenol A, *J. Org. Chem.* 69 (2004) 4724–4731, <https://doi.org/10.1021/jo0356964>.
- [56] H. Xia, H. Tan, H. Cui, F. Song, Y. Zhang, R. Zhao, Z.-N. Chen, W. Yi, Z. Li, Tunable selectivity of phenol hydrogenation to cyclohexane or cyclohexanol by a solvent-driven effect over a bifunctional Pd/NaY catalyst, *Catal. Sci. Technol.* 11 (2021) 1881–1887, <https://doi.org/10.1039/D0CY02188A>.
- [57] I. McManus, H. Daly, J.M. Thompson, E. Connor, C. Hardacre, S.K. Wilkinson, N. Sedaie Bonab, J. ten Dam, M.J.H. Simmons, E.H. Stitt, C. D'Agostino, J. McGregor, L.F. Gladden, J.J. Delgado, Effect of solvent on the hydrogenation of 4-phenyl-2-butanone over Pt based catalysts, *J. Catal.* 330 (2015) 344–353, <https://doi.org/10.1016/j.jcat.2015.06.008>.
- [58] H. Takagi, T. Isoda, K. Kusakabe, S. Morooka, Effects of solvents on the hydrogenation of mono-aromatic compounds using noble-metal catalysts, *Energy Fuels* 13 (1999) 1191–1196, <https://doi.org/10.1021/ef990061m>.
- [59] T.K.H. Trinh, J.C. de Hemptinne, R. Lugo, N. Ferrando, J.P. Passarello, Hydrogen solubility in hydrocarbon and oxygenated organic compounds, *J. Chem. Eng. Data* 61 (2016) 19–34, <https://doi.org/10.1021/acs.jced.5b00119>.
- [60] A. Davis, J.H. Golden, Stability of polycarbonate, *J. Macromol. Sci. Part C* 3 (1969) 49–68, <https://doi.org/10.1080/15583726908545896>.
- [61] Y. Zhang, L. Li, F. Liu, H. Qi, L. Zhang, W. Guan, Y. Liu, A. Wang, T. Zhang, Synergy between Ru and WO<sub>x</sub> enables efficient hydrodeoxygenation of primary amides to amines, *ACS Catal.* 12 (2022) 6302–6312, <https://doi.org/10.1021/acscatal.2c01264>.
- [62] T. Li, N. Ji, Z. Jia, X. Diao, Z. Wang, Q. Liu, C. Song, X. Lu, Effects of metal promoters in bimetallic catalysts in hydrogenolysis of lignin derivatives into value-added chemicals, *ChemCatChem* 12 (2020) 5288–5302, <https://doi.org/10.1002/cctc.202001124>.
- [63] R. Shu, R. Li, Y. Liu, C. Wang, P.F. Liu, Y. Chen, Enhanced adsorption properties of bimetallic RuCo catalyst for the hydrodeoxygenation of phenolic compounds and raw lignin-oil, *Chem. Eng. Sci.* 227 (2020), 115920, <https://doi.org/10.1016/j.ces.2020.115920>.
- [64] J.K. Yu, F. Deng, X. Chen, G. Cheng, Y. Liu, W. Zhang, J.A. Lercher, Impact of hydronium ions on the Pd-catalyzed furfural hydrogenation, *Nat. Commun.* 13 (2022) 7154, <https://doi.org/10.1038/s41467-022-34608-8>.
- [65] A.K. Kar, R. Sarkar, A.K. Manal, R. Kumar, S. Chakraborty, R. Ahuja, R. Srivastava, Unveiling and understanding the remarkable enhancement in the catalytic activity by the defect creation in UiO-66 during the catalytic transfer hydrodeoxygenation of vanillin with isopropanol, *Appl. Catal. B* 325 (2023), 122385, <https://doi.org/10.1016/j.apcatb.2023.122385>.
- [66] N.C. Nelson, J.S. Manzano, A.D. Sadow, S.H. Overbury, I.I. Slowing, Selective hydrogenation of phenol catalyzed by palladium on high-surface-area ceria at



- room temperature and ambient pressure, *ACS Catal.* 5 (2015) 2051–2061, <https://doi.org/10.1021/cs502000j>.
- [67] V. Krishnakumar, M. Kumar, N. Prabavathi, R. Mathammal, Molecular structure, spectroscopic studies (FTIR, FT-Raman and NMR) and HOMO–LUMO analysis of 6-chloro-o-cresol and 4-chloro-3-methyl phenol by density functional theoretical study, *Spectrochim. Acta Part A: Mol. Biomol. Spectrosc.* 97 (2012) 144–154, <https://doi.org/10.1016/j.saa.2012.05.070>.
- [68] G.S. Foo, A.K. Rogers, M.M. Yung, C. Sievers, Steric effect and evolution of surface species in the hydrodeoxygenation of bio-oil model compounds over Pt/HBEA, *ACS Catal.* 6 (2016) 1292–1307, <https://doi.org/10.1021/acscatal.5b02684>.
- [69] J. Zhang, B. Fidalgo, D. Shen, X. Zhang, S. Gu, Mechanism of hydrodeoxygenation (HDO) in anisole decomposition over metal loaded Brønsted acid sites: Density Functional Theory (DFT) study, *Mol. Catal.* 454 (2018) 30–37, <https://doi.org/10.1016/j.mcat.2018.05.015>.